

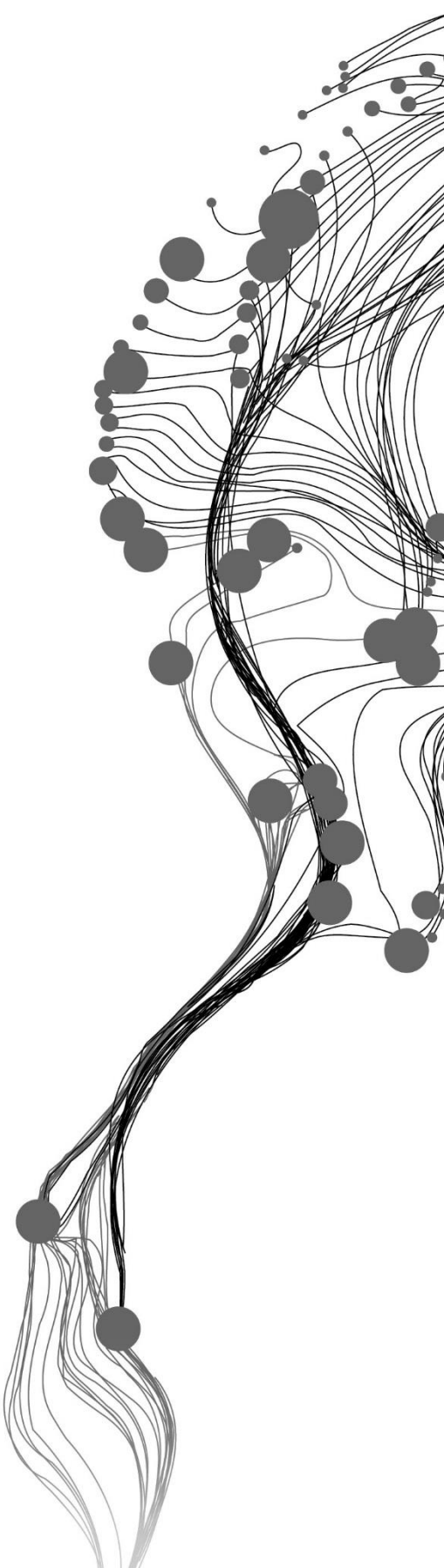
USE OF GOOGLE EARTH ENGINE IN MONITORING AND ANALYZING WETLAND DYNAMICS IN TANGUAR HAOR, BANGLADESH

**MD ZUBAER IMTIAZ HOSSAIN
MARCH 2019**

SUPERVISORS:

Dr. B.H.P. Maathuis

Ir. G.N. Parodi (Gabriel)



USE OF GOOGLE EARTH ENGINE IN MONITORING AND ANALYZING WETLAND DYNAMICS IN TANGUAR HAOR, BANGLADESH

MD ZUBAER IMTIAZ HOSSAIN
Enschede, The Netherlands, [March 2019]

Thesis submitted to the Faculty of Geo-Information Science and Earth Observation of the University of Twente in partial fulfilment of the requirements for the degree of Master of Science in Geo-information Science and Earth Observation.

Specialization: Water Resources and Environmental Management

SUPERVISORS:

Dr. B.H.P. Maathuis

Ir. G.N. Parodi

PROPOSAL ASSESSMENT BOARD:

Dr. ir. Mhd. Suhyb Salama (Chair)

Prof. Dr. R. Zurita Milla, (External Examiner, University Twente)

DISCLAIMER

This document describes work undertaken as part of a programme of study at the Faculty of Geo-Information Science and Earth Observation of the University of Twente. All views and opinions expressed therein remain the sole responsibility of the author, and do not necessarily represent those of the Faculty.

ABSTRACT

Comprehensive monitoring of dynamics indicators of wetlands is embedded inside the clear and timely representation of the stochastic nature of wetland's hydrologic and vegetation regimes. These indicators are change of state of inundation over time in terms of hydrological regime. In terms of vegetation regime dynamics- change of vegetation life form, pattern or percentage of vegetation cover over time act as dynamics indicator. Remote sensing technology offers effective ways to monitor these indicators by providing long-term time series of these indicator related data. Modern advances in cloud computing platform and machine learning algorithms are shifting the way these earth observation data can be utilized in terms of further developments of these dynamic characteristic's analysis. A new emergent cloud-based platform Google Earth Engine can simplify the monitoring and analysis of this dynamics evaluation by providing petabytes scale of publicly available geo-spatial remote sensing data and quick pre-processing combined with spatial analysis in the cloud. Tanguar Haor which is one of the two major Ramsar Sites of the country contains a rich amount of bio-diversity and as well as a highly productive ecosystem is undergoing a radical change in its form over the decades. This dynamic behaviour is particularly of interest during the time period of post monsoon to pre monsoon period of time because in this time period water in the floodplains and inundation regimes get dried up making space for vast levels of Boro rice cultivation throughout the paddy fields there. Utilizing the Google Earth Engine's data storage pre-monsoon to post-monsoon season Sentinel-2 and Land surface reflectance product of Landsat-8 from year 2016-17 and 2017-18 were derived to proceed with the dynamics monitoring. Modified normalized difference vegetation index (MNDWI) and Soil adjusted vegetation index (SAVI) were calculated to look at the dynamics from both hydrologic and vegetation regime perspective respectively. Using Google Earth Engine's application of masking a range of values these indices were used to delineate water and vegetation dynamics from temporal and spatial point of view. These results later were exported to QGIS and ILWIS software for further statistical analysis of dynamics. Results show from 2016-17 to 2017-18 a significant amount of permanent water bodies were lost in the hydrologic regime. In the vegetation regime areas, which always show a high cover percentage of vegetation went through a radical decrease and areas which always show low cover significantly increased. In the transitory water parts where hydrologic regime and vegetation regime both meet the conversion of month to month landcover conversion in those parts were calculated which showed that at the initial period of post monsoon most areas of the wetland were susceptible to change their state from water to soil mixed with water while at the end of dry season or beginning of pre-monsoon season this turned into soil mixed with water to drier soil indicating an initialization of agricultural activities being started there. Locations of different levels of soil state conversion i.e. moist and drier soil and vice-versa from water, was derived from summing post monsoon to pre monsoon period images in ILWIS.

Keywords: Google Earth Engine, wetland dynamics, hydrologic and vegetation regime, spectral index, permanent water and transitory water, data availability

ACKNOWLEDGEMENTS

I enjoyed the support, help and encouragement of many people and institutions within the 18 months programme and in conducting this research. First and foremost, I would thank my supervisor, Dr. B.H.P. Maathuis for his advice and thoughtful suggestions on the work. Your relentless support in conceptualizing the idea for this research is much appreciated. I also thank my second supervisor, Ir. G.N. Parodi (Gabriel), for his encouragement and guidance were instrumental and helpful for finalising this research. I am highly indebted to University of Twente ITC Excellence Scholarship Award that had granted me for my entire study period. I say thank you to ITC for giving me this award in support of my 18 months study for the Water Resources and Environmental Management programme at the Faculty of Geo-Information Science and Earth Observation, University of Twente. My heart goes out to my dear family members for their love, care, support, prayers and encouragement all through this point. Finally, I say thanks to all my classmates and friends of ITC who constantly supported me to get through this challenging period of my life.

TABLE OF CONTENTS

Table of Contents

| | |
|--|-----|
| List of appendices | xi |
| List of acronyms | xii |
| 1. INTRODUCTION..... | 1 |
| 1.1. Research problem | 1 |
| 1.2. Justification | 1 |
| 1.3. Research objectives | 2 |
| 1.3.1. General objectives..... | 2 |
| 1.3.2. Specific objectives | 2 |
| 1.4. Research questions | 2 |
| 2. LITERATURE REVIEW..... | 3 |
| 2.1. Remote sensing of wetland dynamics using optical and radar remote sensing..... | 3 |
| 2.2. Required functionality for wetland dynamic mapping..... | 4 |
| 2.3. Required functionality of Google Earth Engine as a cloud-computing platform in the context of dynamic change monitoring and analysis approaches of wetlands..... | 7 |
| 2.4. Overview of monitoring and analysis approaches in Tanguar Haor wetland, wider context of the topic | 10 |
| 2.5. Comparison of methodological approaches in the context of Google Earth Engine as a cloud-computing platform in terms of wetland dynamics evaluation as a cover of earth surface | 11 |
| 3. METHODOLOGY..... | 13 |
| 3.1. Study area..... | 13 |
| 3.1.1. Geographical location, hydrologic, geomorphic characteristics and river systems | 13 |
| 3.1.2. Method selection for water and vegetation dynamics representation | 14 |
| 3.1.3. Selection of data for monitoring..... | 14 |
| 3.2. Framework of methodology..... | 15 |
| 3.2.1. Flow chart showing the methodology of research | 15 |
| 3.2.2. Image availability inspection..... | 16 |
| 3.2.3. Google Earth Engine functions in terms of water indices calculations | 18 |
| 3.2.4. Thresholding of MNDWI in Google Earth Engine in terms of producing informative datasets..... | 20 |
| 3.2.5. Reclassification | 23 |
| 3.2.6. Exporting images to QGIS..... | 26 |
| 3.2.7. Exporting images to ILWIS | 28 |
| 4. RESULTS | 29 |
| 4.1. Overview of Planet high resolution images used for comparison with thresholded image..... | 29 |
| 4.2. Normal distribution results from November 2017 and comparisons with high resolution image..... | 29 |
| 4.3. Overview of month to month temporal dynamics of hydrological regime MNDWI thresholds and vegetation regime by SAVI thresholds | 31 |
| 4.4. Hydrological and vegetation dynamics explained from above table through thresholding of spectral indices | 34 |
| 4.5. Results from reclassified MNDWI and SAVI mosaics | 35 |

| | | |
|--------|--|----|
| 4.6. | Results from integration of temporal dynamics..... | 37 |
| 4.6.1. | Hydrological regime..... | 37 |
| 4.6.2. | Vegetation regime | 38 |
| 4.7. | Results from November to January cover change showing transitory part of water during 2017-18 to understand transformation from one cover to another over time | 39 |
| 4.8. | Comparison of areas changed between hydrological regime and vegetation regime throughout pre-monsoon to post-monsoon season from 2016-17 to 2017-18..... | 40 |
| 4.9. | Comparison of areas coverages by different conversion type for the year 2017-18 from pre-monsoon to post-monsoon season showing transitory water cover conversion..... | 41 |
| 4.10. | Map showing locations of different levels of susceptibility to water dynamics all derived together in one image..... | 42 |
| 5. | DISCUSSIONS..... | 43 |
| 5.1. | Dynamics of permanent water body, permanent high percentage of vegetated areas..... | 43 |
| 5.2. | Areas covered by different types of cover conversions..... | 43 |
| 5.3. | Different levels of susceptibility of water dynamics throughout the study area | 44 |
| 5.4. | Usage of Google Earth Engine in mapping dynamics of wetlands in the context of this analysis | 45 |
| 6. | CONCLUSIONS AND RECOMMENDATIONS | 46 |
| 6.1. | Conclusions | 46 |
| 6.2. | Recommendations..... | 47 |
| 7. | LIST OF REFERENCES..... | 48 |

LIST OF FIGURES

| | |
|---|----|
| Figure 1 Spectral reflectance of turbid water (Huang et al., 2018) | 5 |
| Figure 2 Spectral reflectance of soil with different levels of soil moisture (Huete, 1992) | 6 |
| Figure 3 Data availability inside Google Earth Engine (Source: Gorelick et al., 2017) | 9 |
| Figure 4: Location of the study area (Source: CEGIS)..... | 13 |
| Figure 5 Methodology showing the work flow..... | 15 |
| Figure 6 Layer visualization tool in GEE..... | 20 |
| Figure 7 Sample polygons taken over a homogenous region to detect normal distribution..... | 22 |
| Figure 8 polygons generated normal distribution..... | 22 |
| Figure 9: Normal distribution range for <0.930 and >0.6..... | 30 |
| Figure 10: Normal distribution for >0.930 | 30 |
| Figure 11 Reclassified image of MNDWI thresholds from November 03, 2017 | 35 |
| Figure 12 Reclassified SAVI image..... | 36 |
| Figure 13: Permanent water bodies of 2017-18..... | 37 |
| Figure 14: Permanent water areas of 2017-18..... | 37 |
| Figure 15: Permanent water bodies that changed from 2016-17 to 2017-18..... | 37 |
| Figure 16: Permanent areas of high vegetation 2016-17 | 38 |
| Figure 17: Permanent areas of high vegetation 2017-18..... | 38 |
| Figure 18: Change of permanent areas of highly vegetated areas from 2016-17 to 2017-18..... | 38 |
| Figure 19: January to March conversion dynamics within post-monsoon to pre-monsoon season delineating further transition from figure-21 | 39 |
| Figure 20: November to January conversion dynamics within post-monsoon to pre-monsoon season delineating transitory parts of Tanguar Haor..... | 39 |
| Figure 21: Amount of change in hydrological and vegetation regime area in square kilometers | 40 |
| Figure 22: Area coverages of water cover conversions | 41 |
| Figure 23: Frequency of different conversion processes occurring throughout the study area. | 42 |

LIST OF TABLES

| | |
|---|----|
| Table 1: Datasets provided in Google Earth Engine..... | 8 |
| Table 2 : Procedure of selecting normal distribution..... | 29 |
| Table 3 Thresholds for November 3 rd image..... | 31 |
| Table 4: Thresholds for January 22 nd image..... | 32 |
| Table 5: Thresholds for March 23 rd image | 33 |

LIST OF APPENDICES

| | |
|---|----|
| Appendix 1: Reclassified MNDWI images..... | 52 |
| Appendix 2 Reclassified SAVI images | 54 |
| Appendix 3: Example of codes to generate one full MNDWI and SAVI calculation..... | 57 |

LIST OF ACRONYMS

| | |
|-------|---|
| API | Application Programming Interface |
| ASTER | Advanced Spaceborne Thermal Emission and Reflection |
| AVHRR | Advanced very High-Resolution Radiometer |
| CEGIS | Centre for Environmental and Geographic Information Service |
| ESA | European Space Agency |
| GEE | Google Earth Engine |
| GUI | Graphical User Interface |
| IUCN | International Union for Conservation of Nature |
| JICA | Japan International Cooperation Agency |
| MNDWI | Modified Normalized Difference Water Index |
| MSI | Multispectral Imager |
| MSS | Landsat Multispectral Scanner |
| MODIS | Moderate Resolution Imaging Spectroradiometer |
| NDVI | Normalized Difference Vegetation Index |
| NDWI | Normalized Difference Water Index |
| NIR | Near Infra-red |
| REST | Representational State Transfer |
| SAR | Synthetic Aperture Radar |
| SAVI | Soil-Adjusted Vegetation Index |
| SRTM | Shuttle Radar Topographic Mission |
| SWIR | Short Wave Infra-Red |
| TCW | Tasseled Cap Wetness Index |
| TIR | Thermal Infra-red |
| VIN | Vegetation Index Number |

1. INTRODUCTION

1.1. Research problem

Tanguar Haor is a multiple-resource base wetland system, supporting a significant combination of rare, vulnerable and endemic species of plants and animals, including major rice growing agriculture and abundant aquatic vegetation providing rich grazing for domestic livestock. Such abundance of natural resources demand for an integrated sustainable monitoring and analysis approach (Karim, Rashid, Sobhan, & Mahmud, n.d.). The dynamic behaviour of the hydrological regime of this haor makes it vulnerable to natural disasters causing this zone of the country still being under developed despite of being one of the major economic production zones also hampering ecological balance there (CEGIS, 2012). An effective monitoring plan taking into consideration the dynamic aspects of the wetland system can ensure in depth study about the impact of unusual changing pattern by identification of key drivers behind this dynamism facilitating optimization of haor monitoring approach (Karim et al., n.d.). Such approach demands for an extensive amount of field studies to be carried out with different instruments for each variable to be calculated and needs a huge amount of workforce and cost.

Hence, remote sensing could come into play in this regard. Satellite images could replace the field work to ensure the data availability for analysis. But such study will need to analyse different types of discrete remote sensing time-series data associated with the wetland dynamics to get an overview from different perspectives. These geo-spatial datasets are scattered around internet at different websites which makes it difficult to blend the information together and conduct any mathematical analysis hindering the path for a comprehensive analysis to be carried out. A big hindrance in the path of such ease of analysis is to identify suitable cloud-free images analysable in an easy way for specific research questions. Moreover, images may vary according to their spatial, spectral, temporal coverage and pre-processed states which create further complications for integration-based calculations. Integration based calculations make wetland monitoring more comprehensive (Alonso, Kennedy, & Murcia, 2016). Besides, such integration requires a lot of time to process let alone in one consolidated system thus obstructing the scope of such researches to be completed within a specified period if any deadline is fixed.

1.2. Justification

The Tanguar haor wetland, was declared as an "Ecologically Critical Area" by the Bangladeshi government in 1999. Many studies have been carried out since then to assess the dynamic changes occurring in this wetland. Whether remote sensing-based analysis or field visit based, most of these studies focused on either hydrologic or vegetation dynamics occurring there to monitor wetland dynamics despite each of them being equally important indicator of this dynamism. Most likely this is because of extensive data requirement needed to focus on both aspects at the same time. Google Earth Engine has never been used here before to do any kind of analysis.

This study thus can bring significant contribution to the scientific community by analyzing applicability of a cloud-based platform Google Earth Engine to monitor and analyze this dynamism by utilizing its functions of solving complexity of extracting and combining different types of remote sensing datasets depicting different information together with one click on the built-in application programming interface with the advantage of petabyte scale parallel computation of geo-spatial time-series thus reducing vast field

measurements and time consumption of computation. The ease of access of pre-processed and geo-referenced data enhances fast-processing. Such illustrative representations of wetland dynamics from the perspective of blended dependency of hydrologic and vegetation regime throughout the study area attributing to the portrayal of the conversion dynamics of the landscape features occurring can provide an informative dataset to be further utilized as a basis for comprehensive management.

1.3. Research objectives

1.3.1. General objectives

The objective in this research is to utilize Google Earth Engine in the context of overarching monitoring of wetland dynamics and inspecting the possibilities of utilizing its functions to analyze these dynamisms.

1.3.2. Specific objectives

- To map inundation dynamics and vegetation dynamics in Tanguar Haor using spectral indices in Google Earth Engine.
- To integrate the inundation and vegetation dynamics maps to get the areas of permanent inundation, transitory waterbody and non-water areas as well as permanent areas of high percentage vegetation cover and low percentage of vegetation cover.
- To use the inundation and vegetation dynamics maps to map the locations and extent of landcover conversion of one type to another.
- To use the inundation maps to map the locations of various levels of susceptibility of water regime landcover conversions.

1.4. Research questions

- 1 What algorithms do Google Earth Engine use to integrate the inundation and vegetation dynamics information to characterize the permanent or transitory water parts?
- 2 From the point of view of change of permanent features from 2016-17 to 2017-18 which regime change had a higher coverage over the study area?
- 3 Which type water cover conversion dominates throughout the transitory parts of the study area?

2. LITERATURE REVIEW

2.1. Remote sensing of wetland dynamics using optical and radar remote sensing

The term “wetlands” covers a wide variety of aquatic habitats, including marshes, swamps, bogs, fens, peatlands, prairie potholes, vernal pools, and aquatic beds, among others. In general, wetlands are transitional habitats situated between wet and dry environments that is saturated with water long enough to promote wetland or aquatic processes as indicated by poorly drained soils, hydrophytic vegetation, and various kinds of biological activity which are adapted to the characteristics of that wet environment. Along the continuum of the water gradient demarcation of wetlands occur and for each demarcated part of these aquatic process triggering elements show distinctive and dynamic behaviours both spatially and temporally. Because of this diverseness in their characteristics there is no single indisputable method of monitoring this dynamic behaviour. Combinative characterization of these diversity specific indicators can assist in identification and delineation of these dynamism for each demarcated part in a comprehensive way (Wu, 2017).

For illustration of the area and distribution of these dynamic characteristics’ remote sensing is a cost-effective tool that can acquire frequent spatial and spectral measurements of high temporal and spatial resolution data-integrated monitoring through various satellite observations in a timely manner. Utilizing this information in the context of dynamics evaluation for both water and vegetation demands for systematic spectral and spatial operations to be performed among these images.

As a source of rapid collection of large amounts of data and unique overview of an area aerial photographs have a vast usage in wetland mapping. These are principle remote sensing technology to analyse ground surface dynamics. Coarse spatial resolutions remote sensing data used in wetland mapping include MODIS and AVHRR data. MODIS has significant applications for wetland mapping wetland extent and dynamics at a coarse spatial resolution. Medium spatial resolution refers to the spatial resolution within the range of 4-30 meters. Medium resolution data mainly includes Landsat TM/Enhanced Thematic Mapper Plus, Landsat Multispectral Scanner (MSS), Advanced Spaceborne Thermal Emission and Reflection Radiometer (ASTER). Because of its higher accuracy and increased number of optical bands for many wetland change detection analysis this data is frequently used (Guo, Li, Sheng, Xu, & Wu, 2017). High resolution satellite data has also been used in wetland remote sensing studies to look at the dynamic information of wetland covers at a smaller scale. Sentinel-2 data has been frequently used to detect dynamic surface processes of earth (Kaplan, Avdan, & Leeuwen, 2017). Optical satellites are mostly effective in wetland vegetation monitoring and wetland change mapping. Synthetic aperture radar (SAR) technology provides significantly important data with its ability to image landscape through cloud cover, day and night, which often can be a limitation for optical sensors. Over the years, SAR data have been successfully used in different land-use/land cover applications. With the launch of the Sentinel-1 mission, a new era for SAR mapping has begun; thus, the use of C-band in monitoring changes and mapping wetlands has increased (Kaplan et al., 2017).

2.2. Required functionality for wetland dynamic mapping

Long period temporal wetness of lands is the first condition to be designated as a wetland which make hydrology the most important controlling factor in terms of regulating the dynamism of formations and functions of wetlands. Based on the frequency and duration of this wetness different stages of changing water cover conditions keep occurring over time which make hydrological regime the most dynamic aspect to be captured in terms of wetland dynamics quantification. Another very distinctive behaviour of wetland includes its dynamic colonization of the wetland with various life forms, patterns and density in a very rapid manner. These plants are called hydrophytic vegetation which have integrated with the frequency and duration of inundation behaviour of wetlands (Wu, 2017). These two aspects being the most changing indicator of wetland dynamism can control the flood peaks by decolonizing currents of water and flood peaks.

Density slicing of specific operation related band information, land cover maps generated from supervised or unsupervised classification can derive dynamic characteristics of wetland. However, these methods are difficult to build and are not universally acceptable (Huang, Chen, Zhang, & Wu, 2018). An often-used approach to study temporal changes is to summarize their spectral information by transforming spectral data using ratios between bands to reduce the data into meaningful information (Muñoz et al., 2015). Many indices have been developed to extract surface water areas or flood inundation extent. For example, Crist (1985) proposed the Tasseled Cap Wetness (TCW) index derived from six bands of surface reflectance data and set a threshold of 0 to separate water and nonwater objects. Normalized difference vegetation index (NDVI), which is a vegetation index, has been used to detect water and flood in some studies. More useful indices for this purpose are those that can better highlight water bodies, such as normalized difference water index, and modified NDWI. McFeeters's NDWI can be regarded as the first generation of water index. Later, Xu (2006) found that the Short-wave Infrared (SWIR) band can reflect some subtle characteristics of water, and so replaced the Near Infrared (NIR) band in NDWI with the SWIR band and proposed the MNDWI. It is now widely accepted that MNDWI is more stable and reliable than NDWI, because the SWIR band is less sensitive to concentrations of sediments and other optical active constituents within the water than the NIR band is. Therefore, MNDWI has been widely used in many recent studies.

Spectral reflectance of water is controlled by mainly four factors i.e. turbidity of water, chlorophyll concentration of water, depth of water and substrate below the water (Ma et al., 2019). MNDWI values are created utilizing the spectral response of Green band and Short wave infra-red band to water and non-water features. Hence sensitivity of these two bands to above mentioned conditions of water if can be linked with reliable proofs that can be used to label different conditions of water per month according to the threshold ranges. Further the label information can be compared with interpretation of high-resolution imageries for proof.

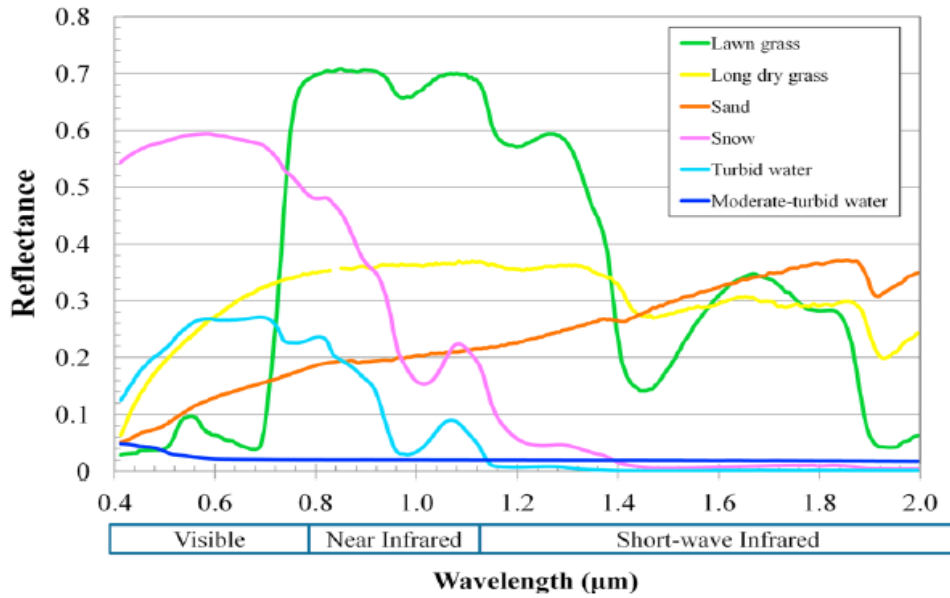


Figure 1 Spectral reflectance of turbid water (Huang et al., 2018)

Hence, MNDWI for turbid water and less turbid water can be calculated according to the reflectance values mentioned in figure-1

$$MNDWI_{turbid} = \frac{0.32-0}{0.32+0} = 1 \dots\dots\dots (1)$$

The values show for very high turbid water the value can be as high as 1, as turbid water doesn't show any reflectance in Short wave infra-red region.

In less turbid water the reflectance decreases rapidly in green band region but reflectance in short-wave infra-red region increases slightly. Increase in green band region in case of turbid water may be caused by different reasons i.e. sediments, pollutants, phytoplankton, and other materials present in water which increase the reflectance in green band (Huete, 1992). In clearer water reflectance in green band decreases rapidly because of decrease in green band reflective constituents present in water. Hence, every level decrease from very high value of MNDWI to low value of MNDWI could be linked to different levels of decrease in turbidity levels. This is one possibility. As sensitivity of chlorophyll concentration to green band and SWIR band is less reliable than red and Near Infrared band but sensitivity of sediments to green and SWIR band is more reliable hence separate ranges could be interpreted as from different turbidity levels (Murat & Ceylan, 2005). All this information together could be used as the temporal dynamics' indicator of water part of a wetland.

In terms of predicting about depth and bottom features of water Sentinel-2 TOA reflectance of green band and SWIR band is not sufficient (Dörnhöfer, Göritz, Gege, Pflug, & Oppelt, 2016). (Huete, 1992) showed that with increasing effect of water on soil reflectance make soil darker when moistened, particularly in the shortwave infrared region (1.45-1.9 micrometers).

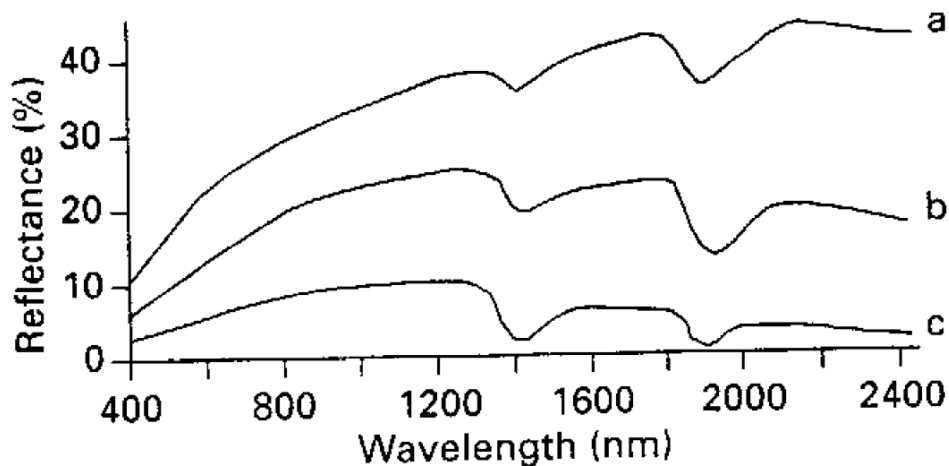


Figure 2 Spectral reflectance of soil with different levels of soil moisture (Huete, 1992)

In figure-2, a, b and c respectively indicate reflectance behaviour of soil with 5, 20 and 40% of water content. With increasing amount of water content, the reflectance tends to decrease. But while comparing the green band and SWIR region we can see with every level of increase in water content decrease in SWIR region is more rapid and high in quantity comparing the green band region. Here with 40% water content the SWIR region reflectance is greater than the green band region hence the MNDWI value will be negative. But from the rapidness of decrease in SWIR region because of water content increase in soil indicate that with further increase the value of SWIR region will decrease more and maybe it would be smaller than the green band. Because with 40% water SWIR reflectance is only slightly higher than the green band reflectance. Hence, any value of MNDWI less than the previous assumption (0.333) could be linked with different levels of soil moisture.

Besides, (Singh, Prasad, Pateriya, Sahoo, & Setia, 2014) showed that MNDWI value for water features mixed with vegetation has a value of 0.28. Hence, values less than 0.28 can be labelled as soil with different levels of soil moisture and 0.28 to 0.3 as waterlogged areas with vegetation and anything greater than 0.3 as different levels of turbidity.

In terms of vegetation dynamics quantitative and qualitative evaluation of vegetative cover change have been monitored through the usage of vegetation indices calculated from spectral indices. These indices can be utilized to understand the dynamics of vegetation from different aspects such as vegetation cover density, crop discrimination, land use changes according to the interest of the researcher. The different vegetative covers can be distinguished according to their unique spectral behaviour in relation to overall ground elements. Green vegetation shows a step-function curve due to pigment absorption in the red and scattering of incident radiation in the NIR whereas non-green materials show a featureless, monotonically increasing signal. The combination of these two spectral domains permits to differentiate vegetation from soils and to determine photosynthetically active biomass through vegetative cover density which depicts the percentage of vegetation cover density (Nagler, Glenn, & Huete, 2001). Pearson and Miller (1972) are pioneers in the history of vegetation indices. They developed the first, two indices in the form of ratios: the "Ratio Vegetation Index" (RVI) and the "Vegetation Index Number" (VIN), Rouse et al. (1974) proposed the "Normalized Difference Vegetation Index" (NDVI): using red and near infra-red channel of Landsat. The index is sensitive to the presence of green vegetation it permits the prediction of agricultural crops (Bannari, Morin, Bonn, & Huete, 1995). But these indices are contaminated with the background effects of soil for a

given amount of vegetation, darker soil substrates resulted in higher vegetation index values when the ratio vegetation index were used as measures. Soil Adjusted Vegetation Index (SAVI) is an arithmetic adjustment of NDVI index can minimize this effect of background soil on vegetation indexes for dynamics mapping (A. R. HUETE, 1988).

2.3. Required functionality of Google Earth Engine as a cloud-computing platform in the context of dynamic change monitoring and analysis approaches of wetlands

Combinative use of remote sensing monitoring results can create scopes for derivation of innovative process-analysing algorithms (Kabisch, Selsam, Kirsten, Lausch, & Bumberger, 2019). Utilization of these algorithms in a systematic manner with a view to expanding the objectives of comprehensive potentiality of algorithm results, emergence of innovative depiction of these dynamic earth processes may be possible.

Dynamics in the context of wetland as a surface cover of the earth can be recognized by the change of extent and rate of conversion from one wetland land cover type i.e. transitional state of inundation to vegetative cover, saturated soil condition or any other cover type over time (Mitsch & Gosselink, n.d.). Comprehensive monitoring programmes giving time-series information regarding location of water and vegetation occurrence, extent and natural variability of these cover types is the basis of this dynamics evaluation (Hird, Delancey, & Mcdermid, 2017). However, ground-measured time series of these variables are often not readily available due to the tediousness of the work and the financial and time investment required, especially for large-scale wetland systems (Alonso et al., 2016). Besides, the volume and speed of analysing of these time-series data that is needed to monitor and analyse this dynamism is out of reach of traditional computing machine's storage and calculation ability (Wang, Wang, Chen, & Ni, 2013). Further, the variety in format and spatiotemporal resolution of these dynamics data make it difficult to find an easy-to-use tool to analyse this dynamism together in a rapid manner (Yang, Yu, Hu, Jiang, & Li, 2017). These problems hinder the possibility of achieving comprehensiveness of the process-analysing algorithms which could take depiction of wetland dynamics one step further without carrying out any field measurement in a cost-effective manner.

Cloud-computing is an internet-based supercomputing paradigm providing a form of utility through enabling ubiquitous, convenient, on-demand network access to a shared pool of configurable computing resources (e.g., networks of wetland remote sensing product storages, applications, parallel processing-based algorithms and services) that can be rapidly processed with minimal management effort, resource pooling and rapid elasticity (Tang & Feng, 2017). Emergence and advancement of free clouds as a satellite product processing platform thus can overcome the complexities involved in storage-related problems and calculation of different file formats and spatio-temporal resolutions satellite products together in a cost-effective and time-saving manner, regarding any type of analysis of the earth's cover (Wang et al., 2013).

Google Earth Engine is a new technology cloud-computing platform that enables monitoring and measurement of earth surface processes via observations from a variety of satellite and aerial imaging systems in both optical and non-optical wavelengths, environmental variables, weather and climate forecasts and hindcasts, land cover, topographic and socio-economic datasets in addition with intrinsically-parallel computational access over these datasets (Gorelick et al., 2017). Earth Engine currently hosts online nearly the complete historical Landsat archive of L5 and L7 data collected over more than twenty-five years. Other satellite sensors offering open-access data sets that complement Landsat are also available (e.g., Advanced Very High-Resolution Radiometer (AVHRR), Advanced Spaceborne Thermal Emission and Reflection Radiometer (ASTER), Shuttle Radar Topography Mission (SRTM)). More recently, the European Space Agency's Sentinel satellite series have begun offering high-resolution EO data related to hydrological and

vegetation regime of a wetland at frequent intervals, representing important extensions to existing data streams (Hird et al., 2017). Combining this massive data and technology resources, GEE supports generation of on-demand, spatial and temporal cloudless mosaics & composites as well as a variety of spectral indices that can facilitate derivation of different dynamic aspects of wetlands. These data are accessible through a high-speed API that allows scientists access to these computational and data resources and scale their current algorithms or develop new ones in an innovative way in one consolidated system of common spatial geo-reference determined by the output resolution, hence ensuring ease-of-use and collaboration of datasets, as well as transparency in data and methods. This study focuses on utilizing wetland-related datasets among these along with its unique functionality of calling data regardless of time and space this platform advances the broader operational deployment of existing scientific methods and strengthens their ability on improved monitoring and analysis of wetland dynamism.

The Earth Engine public data catalogue is a multi-petabyte curated collection of different streams each of which are subdivided into different types based on different types of Earth-observing remote sensing principles of capturing the data such as-

Table 1: Datasets provided in Google Earth Engine

| Data stream | Data types |
|---------------------|-------------------------|
| Climate and weather | Surface temperature |
| | Climate |
| | Atmospheric |
| | Weather |
| Imagery | Landsat |
| | Sentinel |
| | Modis |
| | High resolution imagery |
| Geophysical | Terrain |
| | Landcover |
| | Cropland |
| | Other geophysical data |

The bulk of the catalogue is made up of Earth-observing remote sensing imagery, including the entire Landsat archive as well as complete archives of data from Sentinel-1 and Sentinel-2, but it also includes climate forecasts, land cover data and many other environmental, geophysical and socio-economic datasets (Table 1). The catalogue is continuously updated at a rate of nearly 6000 scenes per day from active missions, with a typical latency of about 24 h from scene acquisition time. Users can request the addition of new datasets to the public catalogue, or they can upload their own private data via a REST interface using either browser-based or command-line tools and share with other users or groups as desired (Gorelick et al., 2017).

An overview of data along with the satellite information present in the Earth Engine archive is shown below-

Frequently used datasets in the earth engine data catalog.

| Dataset | Nominal resolution | Temporal granularity | Temporal coverage | Spatial coverage |
|--|--------------------|----------------------|-------------------|------------------|
| Landsat | | | | |
| Landsat 8 OLI/TIRS | 30 m | 16 day | 2013–Now | Global |
| Landsat 7 ETM + | 30 m | 16 day | 2000–Now | Global |
| Landsat 5 TM | 30 m | 16 day | 1984–2012 | Global |
| Landsat 4–8 surface reflectance | 30 m | 16 day | 1984–Now | Global |
| Sentinel | | | | |
| Sentinel 1 A/B ground range detected | 10 m | 6 day | 2014–Now | Global |
| Sentinel 2A MSI | 10/20 m | 10 day | 2015–Now | Global |
| MODIS | | | | |
| MOD08 atmosphere | 1° | Daily | 2000–Now | Global |
| MOD09 surface reflectance | 500 m | 1 day/8 day | 2000–Now | Global |
| MOD10 snow cover | 500 m | 1 day | 2000–Now | Global |
| MOD11 temperature and emissivity | 1000 m | 1 day/8 day | 2000–Now | Global |
| MCD12 Land cover | 500 m | Annual | 2000–Now | Global |
| MOD13 Vegetation indices | 500/250 m | 16 day | 2000–Now | Global |
| MOD14 Thermal anomalies & fire | 1000 m | 8 day | 2000–Now | Global |
| MCD15 Leaf area index/FPAR | 500 m | 4 day | 2000–Now | Global |
| MOD17 Gross primary productivity | 500 m | 8 day | 2000–Now | Global |
| MCD43 BRDF-adjusted reflectance | 1000/500 m | 8 day/16 day | 2000–Now | Global |
| MOD44 veg. cover conversion | 250 m | Annual | 2000–Now | Global |
| MCD45 thermal anomalies and fire | 500 m | 30 day | 2000–Now | Global |
| ASTER | | | | |
| L1 T radiance | 15/30/90 m | 1 day | 2000–Now | Global |
| Global emissivity | 100 m | Once | 2000–2010 | Global |
| Other imagery | | | | |
| PROBA-V top of canopy reflectance | 100/300 m | 2 day | 2013–Now | Global |
| EO-1 hyperion hyperspectral radiance | 30 m | Targeted | 2001–Now | Global |
| DMSP-OLS nighttime lights | 1 km | Annual | 1992–2013 | Global |
| USDA NAIP aerial imagery | 1 m | Sub-annual | 2003–2015 | CONUS |
| Topography | | | | |
| Shuttle Radar Topography Mission | 30 m | Single | 2000 | 60°N–54°S |
| USGS National Elevation Dataset | 10 m | Single | Multiple | United States |
| USGS GMTED2010 | 7.5° | Single | Multiple | 83°N–57°S |
| GTOPO30 | 30° | Single | Multiple | Global |
| ETOPO1 | 1° | Single | Multiple | Global |
| Landcover | | | | |
| GlobCover | 300 m | Non-periodic | 2009 | 90°N–65°S |
| USGS National Landcover Database | 30 m | Non-periodic | 1992–2011 | CONUS |
| UMD global forest change | 30 m | Annual | 2000–2014 | 80°N–57°S |
| JRC global surface water | 30 m | Monthly | 1984–2015 | 78°N–60°S |
| GLCF tree cover | 30 m | 5 year | 2000–2010 | Global |
| USDA NASS cropland data layer | 30 m | Annual | 1997–2015 | CONUS |
| Weather, precipitation & atmosphere | | | | |
| Global precipitation measurement | 6° | 3 h | 2014–Now | Global |
| TRMM 3B42 precipitation | 15° | 3 h | 1998–2015 | 50°N–50°S |
| CHIRPS precipitation | 3° | 5 day | 1981–Now | 50°N–50°S |
| NLDAS-2 | 7.5° | 1 h | 1979–Now | North America |
| GLDAS-2 | 15° | 3 h | 1948–2010 | Global |
| NCEP reanalysis | 2.5° | 6 h | 1948–Now | Global |
| ORNL DAYMET weather | 1 km | Annual | 1980–Now | North America |
| GRIDMET | 4 km | 1 day | 1979–Now | CONUS |
| NCEP global forecast system | 15° | 6 h | 2015–Now | Global |
| NCEP climate forecast system | 12° | 6 h | 1979–Now | Global |
| WorldClim | 30° | 12 images | 1960–1990 | Global |
| NEX downscaled climate projections | 1 km | 1 day | 1950–2099 | North America |
| Population | | | | |
| WorldPop | 100 m | 5 year | Multiple | 2010–2015 |
| GPWv4 | 30° | 5 year | 2000–2020 | 85°N–60°S |

Figure 3 Data availability inside Google Earth Engine (Source: Gorelick et al., 2017)

2.4. Overview of monitoring and analysis approaches in Tanguar Haor wetland, wider context of the topic

Tanguar Haor is a bowl-shaped natural inland freshwater wetland filled with water formed during monsoon and is comprised of several individual permanent low-lying depressions, acting as a complex of both lakes and marshes depending on its hydraulic behaviour in different seasons. Composed of a rich amount of biodiversity as well as a highly productive ecosystem Tanguar Haor is the largest wetland in the north-eastern region of Bangladesh which has been undergoing a radical change in its form over the decades because of frequent occurrence of natural disasters like flash floods (Haque & Basak, 2017). Flash flood is the main natural disaster here which engulfs the primary production sector (e.g. agriculture) and thus threatens the lives and livelihoods of the inhabitants of the haor region (CEGIS, 2012).

Tanguar Haor is also recognized as a Ramsar site of international importance (Chandra, 2017). The Convention on Wetlands, also known as the Ramsar Convention, is a global inter-governmental treaty that provides the framework for national action and international cooperation for the conservation and wise use of wetlands and their resources. It is the only global treaty to focus on one single ecosystem. The Ramsar Convention on Wetlands has recently been emphasizing development and promotion of guidance and tools for the inventory, assessment and monitoring of change in wetlands with an emphasis on the application of an increasing number of Earth Observation (EO) or satellite-based remote sensing approaches. This includes different approaches as the GEO-Wetlands1, a collaborative framework for international cooperation, co-designing of EO solutions, GlobWetland Africa a tool for wetland mapping and so on. This has become necessary as there is an increasing demand for information that can be readily used by wetland managers to understand and address the ongoing loss and degradation of wetlands, as well as information which can be used to address reporting requirements at the national and international level. Till now in the context of assessment of information needs for wetland management through EO-based remote sensing approach, many case studies have been carried out with the aim of wetland dynamics monitoring and analysis. Such as updating of ecological information on an existing Ramsar Site, Lake Burullus, Egypt, regional extent and trends of Mediterranean wetland status, delineation, physical features of the site and catchment, wetland types, wetland dominance and ecological features of Lake Volta and Lake Victoria, mangrove mapping and change assessment and so on. But still despite being a Ramsar Site, no such studies in terms of information assessment has been carried out in Tanguar Haor, Bangladesh.

Apart from the context of Ramsar Convention site many researches have been carried out in regards of wetland change monitoring and analysis approaches in Tanguar Haor from the educational point of view. Usually wetland monitoring plans are proposed in accordance with the measuring progress towards the stated objectives according to the restoration plan (Comer et al., n.d.). With a view to ensuring better ecosystem management in Tanguar Haor dynamic changes of resource availability were identified through an interview based data collection monitoring method (Miah, Afrad, Mehraj, & Mandal, 2015). In another study, monitoring was carried out through blending of interview-based primary data collection and usage of secondary satellite data, later leading to a spectral indices-based post classification approach with a view to delineating areas of rapid change, magnitude of change and better understanding of dynamics of land cover and trend of change (Haque & Basak, 2017). To find out the dynamic characteristics of phytoplankton communities in Tanguar Haor (Muzaffar & Ahmed, 2007) variation of flood cycles and physiochemical variables were monitored and analysed through a blending of field study and statistical approach.

Most of the studies regarding dynamism in Tanguar Haor are based on field studies or land cover change detection. Because of extensive field data requirements and complexity being arisen from the time-consumption of managing large time-series remote sensing images, over-arching change assessment information evaluation have always been skipped. Usage of a cloud-computing platform has never been

evaluated before in the change assessment of Tanguar Haor. This study focuses on evaluating the usage of a cloud-computing platform Google Earth Engine in terms of gathering change assessment information in an over-arching manner looking at both hydrologic and vegetational cover dynamics there adding to the archival information of Ramsar Site convention.

2.5. Comparison of methodological approaches in the context of Google Earth Engine as a cloud-computing platform in terms of wetland dynamics evaluation as a cover of earth surface

Characterizing wetlands and their dynamics over a large geographical region has been investigated using different techniques with varying degrees of success. Object-based approaches have been applied considering landscapes as aggregation of meaningful objects corresponding to ground entities and patches of vegetation cover to look at the dynamics over time (Nagler et al., 2001). (Papa, Prigent, Durand, & Rossow, 2006) using the passive microwave land surface emissivity detected inundation to quantify spatial and temporal hydrological dynamics. (Yuan, Jiang, Luo, He, & Liu, 2014) quantified wetland area, rate of change and landscape indexes comparing with one image from one period and another image from another period to quantify the dynamics. (Alonso et al., 2016) used spatially aggregated vegetation index time series in Google Earth Engine to provide insight opportunities in wetland's spatio-temporal degradation dynamics. (Nhamo, Magidi, & Dickens, 2017) used an integrative approach of spectral index calculation NDWI and Digital elevation model to monitor the spatio-temporal changes of wetlands over time. SAR data can be used for detecting water dynamics of wetlands through different methods i.e. either by multi-temporal interferometric coherence or by using the texture and local tone based segmentation over time (White, Brisco, Dabboor, Schmitt, & Pratt, 2015).

Usage of Google Earth Engine in terms of reliable earth surface dynamics evaluation i.e. wetlands has been evaluated previously in different research papers. (Midekisa et al., 2017) used Landsat satellite observation data and GEE cloud platform to map land cover and impervious surface changes over continental Africa for 2000 to 2015. He created annual cloud-free composites using a cloud-screening algorithm and calculated annual normalized difference vegetation index (NDVI) and normalized difference water index (NDWI) and took the median value from 3-year windows to analyse the change. (Sidhu, Pebesma, & Câmara, 2018) analyse Singapore's land use and cover through observing the change in Singapore's landmass through land reclamation. They used MapReduce architecture to handle query of land-related datasets, then overlaying raster and vector data to create visualizations following by calculation of generation of EVI charts within the GEE application processing interface (API) for two study areas, namely, Tuas industrial zone and the CCR, focusing on challenges associated with running temporal aggregations and highlighting the "cost of research friendliness" through the generation of runtime statistics for processes within GEE. (Mahdianpari et al., 2018) aims to develop a multi-temporal classification approach based on open-access remote sensing data and tools to map wetland classes as well as the other land cover types with high accuracy, here piloting this approach for wetland mapping in Canada using open access SAR and optical images obtained from Sentinel-1 and Sentinel-2 sensors for the classification of wetland complexes. They also assessed the capability of the Google Earth Engine cloud computing platform to generate custom land cover maps, which are enough in discriminating wetland classes as standard land cover products by comparing the efficiency of both pixel-based and object-based random forest classification thus producing the first provincial-scale, fine resolution (i.e., 10 m) wetland inventory map in Canada. (Alonso et al., 2016) used Landsat and MODIS sensors and available in the GEE cloud, to discriminate the most appropriate images to generate the final vegetation time series, and discuss their initial implications for the study of human degradation of the protected Palo Verde wetland by calculating vegetation index NDVI. (Hird et al., 2017)

by using optical and radar variables and topographic inputs to develop and pilot a reproducible, scalable, machine learning-based approach to the large-area mapping of wetland probability of occurrence.

This study focuses on analysing the capability of Google Earth Engine in the context of using Sentinel-2 data to map hydrological and vegetation dynamics through calculation and thresholding of different spectral indices values and searching for innovative functionality of Google Earth Engine to utilize them to understand the underlying processes of this dynamics.

3. METHODOLOGY

3.1. Study area

3.1.1. Geographical location, hydrologic, geomorphic characteristics and river systems

Tanguar Haor is a leading internationally significant freshwater wetland situated at the north-eastern part of Bangladesh situated between 25°12' 2.572" and 25°5'47.989" North Latitude and 90° 58' 49.426" and 91°10'0.018" East Longitude. The *haor* territory spans over 9500 hectares (‘Information Sheet on Ramsar Wetlands (RIS)’, 2000). It shares a border of approximately 17 km with Nongstoin (Meghalaya), India in its north. Fig. 2 shows the location of Tanguar haor and its surroundings. The haor is located at an altitude of only 2.5–5.5 m above mean sea level. The landscape topography of Tanguar Haor is uneven. Because of its bowl shape nature, it acts like a natural reservoir. The Haor consist of 46–50 beels of various sizes. Within 9500 hectares 2802.36 ha are permanent waterbodies. Total river area within the Tanguar Haor is 359.39 ha. Tanguar Haor act as the flood plain complex of Surma-Kushiyara river system. These two rivers are important tributaries of Meghna River and connected with Dhanu, Baulai and Jadukata River through the extended floodplain of Tanguar Haor (Haque & Basak, 2017). The *haor* system is mainly rendered with the back-water flow of river waters from the Baulai, Patlai and Jadukata rivers. Few hills streams flow into the *haor* system but the major water thrust comes from the south because of the back flow. Because of the low quantity of silt plus its dissemination during flooding season, this *haor* is still deep enough compared to the other *haors* where the rate of sedimentation is comparatively higher (‘Tanguar Haor Management Plan Framework and Guidelines’, n.d.). Some important characteristics of the research area relevant to this study is described in the following sections. The deep blue lines show rivers in the wetland and the pale blue areas show the permanent and temporary stagnant waterbodies which are basically making up the wetlands.

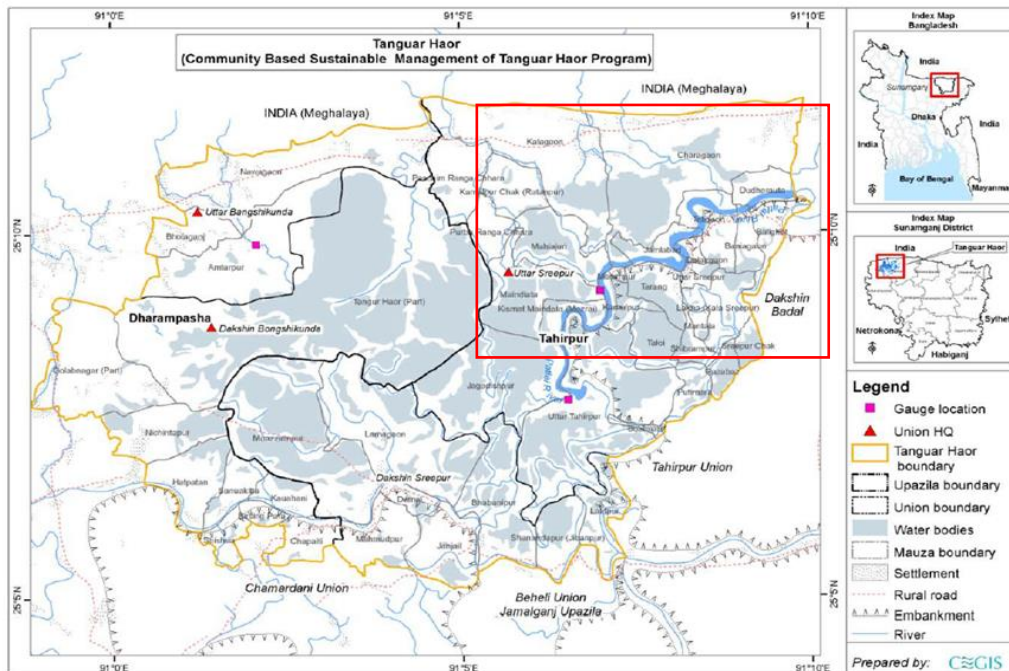


Figure 4: Location of the study area (Source: CEGIS)

3.1.2. Method selection for water and vegetation dynamics representation

The principle of extracting surface water from optical images is the lower reflectance of water, compared to that of other land cover types, in infrared channels. Based on this, many methods have been developed for extracting water areas from optical remote sensing imagery. The easiest and effective among them is to use water indices which are calculated from two or more bands, to distinguish between the water and non-water areas. Among all the spectral indices Normalized difference water index and modified normalized difference water index are the most common and effective water indices for this application, which also selected to be used in our analysis to represent the water dynamics of Tanguar Haor (Huang et al., 2018). In the context of assessing vegetation dynamics usage of vegetation indices is a very common method. For this analysis Soil Adjusted Vegetation Index was chosen to detect the dynamics of vegetation in the study area (Silleos, Alexandridis, Gitas, & Perakis, 2006).

3.1.3. Selection of data for monitoring

High spatial and temporal resolution optical satellite sensors are very useful to capture and resist unfavourable field conditions at the sub-field scale dynamics detection (Han et al., 2017). Sentinel-2 is a satellite launched in 2016 by the European Space Agency (ESA) that carries the Multispectral Imager (MSI) instrument, which captures 12 optical bands at varying spatial resolutions: the three visible bands and the NIR band are available in 10 m resolution; the two SWIR, three red edge bands and narrow-band NIR in 20 m resolution; and coastal aerosol, cirrus and water vapour bands at 60 m resolution (Masiliūnas, Verbesselt, & Pena-Claros, 2017). The Sentinel-2 products are available from the Earth Engine data catalogue at the Level 1C processing level (top-of-atmosphere radiance). Coarse spatial resolution images are unable to detect smaller size open water bodies. Besides, SWIR range which is the best band for distinguishing between water and non-water features, for Sentinel-2 this range of SWIR is narrower than other satellite images. Hence, for water dynamics detection Sentinel-2 Top of Atmosphere cloud free time series data of 2016-17 and 2017-18 these two-year periods of pre-monsoon (November) to end of dry season (March) was used for analysis.

While looking at water & vegetation temporal dynamics through spectral index values this needs very robust atmospheric correction (Silleos et al., 2006). In Google Earth Engine Landsat surface reflectance products being corrected for atmospheric correction is directly provided which are selected for SAVI calculation. Same time period images were used to create a link between these two sets of images. These images contain 4 visible and near-infrared (VNIR) bands and 2 short-wave infrared (SWIR) bands processed to orthorectified surface reflectance, and one thermal infrared (TIR) band processed to orthorectified brightness temperature. The VNIR and SWIR bands have a resolution of 30m / pixel. The TIR band, while originally collected with a resolution of 120m / pixel (60m / pixel for Landsat 7) has been resampled using cubic convolution to 30m.

3.2. Framework of methodology

3.2.1. Flow chart showing the methodology of research

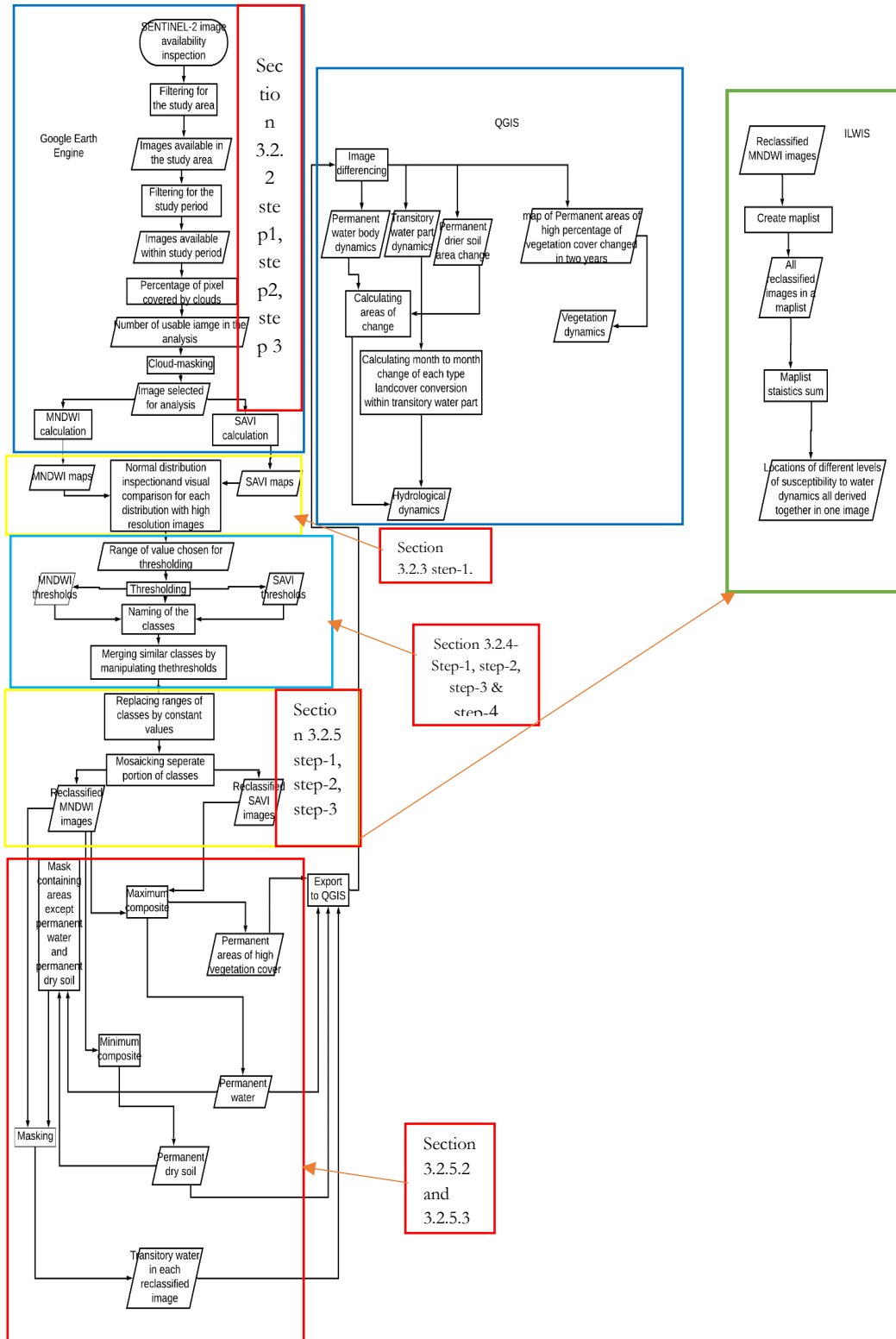


Figure 5 Methodology showing the work flow

3.2.2. Image availability inspection

Earth Engine provides images produced by a single sensor, grouped together as a “collection” known as `imagecollection`. It also allows users to define a point or polygon anywhere on the planet and filter `imagecollection` data from each satellite for user-defined time frames, area extent or location, what percentage of an image pixels inside the `imagecollection` is contaminated by cloud interference and options of predefined or custom image band combinations in compliance with the objective and research question via a simple graphical user interface (GUI) using the function- `.Filter()`.

A script was created to check the cloud-free availability of images starting from November 2017 to March 2018. The scripts is explained below

Step-1. Creating an area of interest only within which the availability of images will be checked.

Script-1 `var tanguarhaor = ee.Geometry.Polygon([`

```
[[[90.9952, 25.16], [91.2616,25.1824],[91.4841,25.1053],[91.55, 24.9647], [91.4594, 24.8065], [90.8772,
24.814],[90.781,24.9635],[90.8043,25.1103],[90.9952,25.16]]
]);
```

- This allows creating a polygon within the specified co-ordinates.
- The projection of this geometry. The default is the projection of the inputs, where Numbers are assumed to be EPSG:4326.

Step-2. Creating a function to masking out clouds over an image collection

Script-2 `function maskS2clouds(image) {`
`var qa = image.select('QA60');`
`var cloudBitMask = 1 << 10;`
`var cirrusBitMask = 1 << 11;`
`var mask = qa.bitwiseAnd(cloudBitMask).eq(0).and(`
`qa.bitwiseAnd(cirrusBitMask).eq(0));`
`return image.updateMask(mask).divide(10000)}`

- Earth engine operates functional programming i.e. mathematical operations without the problem of changing variables each time. Here this function ‘`maskS2clouds`’ is defined as a variable name of a function which is being applied to every image of an image collection by (`image`) call.
- This function goes inside of every Image of an image collection, chooses the ‘QA60’ band which is the cloud mask of sentinel-2 image.
- QA60 has two bits- bit10 and bit11, this `cloudbitmask` goes inside bit 10 and `cirrusbitmask` goes inside bit11 Then through the left operand operation specified ‘<<’ it goes inside every binary digit of both bits.

Step-3. Checking number of cloud-free images available within the specified polygon previously for a specified date range for a specific sensor.

Script-3 `var start = ee.Date('2016-12-01');`
`var finish =ee.Date('2016-12-30');`
`var Tahirpur = ee.ImageCollection('COPERNICUS/S2')`

```
.filterBounds(tanguarhaor)
.filterDate(start,finish)
.filter(ee.Filter.lt('CLOUDY_PIXEL_PERCENTAGE', 1))
.map(maskS2cloud)
print (Tahirpur);
```

- Start and finish indicates the range of date for which availability of images will be checked
- ee.ImageCollection('COPERNICUS/S2') specifies imagecollection of sentinel-2 images.
- .filterBounds() this limit the number of results to be found only within the study area
- .filterDate() limits the number of results within the date range.
- .filter(ee.filter.lt()) limits the number of results if the percentage of pixels being covered by clouds exceed 1 %.
- .map() function applies this maskS2clouds function to every image available inside an image collection and only takes out the pixels that are cloud free.
- In the console tab number of images are printed by the print function.
- By going through each binary digit, it compares each bit of the cloudbitmask with the cirrusbitmask and if both of their value is zero then it specifies a cloud-free pixel and specifies a 1. Otherwise zero. And a mask is created which is later used by an 'updatemask' function to pull out only the cloud-free pixels and divided by 10000 to get the reflectance values in range of 0 to 0.3.

To perform above functions of data inference GEE doesn't require to follow a certain schema for loading data which improves its data inference speed. Even a long time series of data can be displayed in code editor based on a specific criterion though the usage of a few lines of code only within few seconds. Simplified code structure and the bypass of internet traffic or machine failures can be avoided by this functionality of GEE. The data catalogue is attributed with indexing functionality which makes the data calls by user simplified and application based as such in this case we used cloud-free Sentinel-2 data, for an area in Bangladesh, for a specific time period all these criteria is analysed by Google Earth Engine in a very swift way and it gives back the optimized result within a few minutes which would be a tedious work in other software.

List of available images with their ID and metadata is given below-

| Sentinel-2 ImageID (2016-17) | Sentinel-2 ImageID (2017-18) | Landsat 8 Surface Reflectance ImageID (2016-17) | Landsat 8 Surface Reflectance ImageID (2017-18) |
|--|--|---|---|
| 20161113T043032_20161113T043537_T46RCN | 20171103T042919_20171103T043722_T46RCN | LANDSAT/LC08/C01/T1_SR/LC08_137043_20161114 | LANDSAT/LC08/C01/T1_SR/LC08_137043_20171101 |
| 20161123T043112_20161123T043400_T46RCN | 20171223T043159_20171223T043613_T46RCN | LANDSAT/LC08/C01/T1_SR/LC08_137043_20161216 | LANDSAT/LC08/C01/T1_SR/LC08_137043_20171203 |
| 20161223T043202_20161223T044035_T46RCN | 20171228T043201_20171228T044000_T46RCN | LANDSAT/LC08/C01/T1_SR/LC08_137043_20170117 | LANDSAT/LC08/C01/T1_SR/LC08_137043_20180309 |
| 20170211T042911_20170211T043113_T46RCN | 20180122T043059_20180122T043855_T46RCN | LANDSAT/LC08/C01/T1_SR/LC08_137043_20170218 | |
| | 20180201T043009_20180201T043008_T46RCN | | |
| | 20180216T042841_20180216T042842_T46RCN | | |
| | 20180308T042701_20180308T043336_T46RCN | | |
| | 20180323T042659_20180323T044040_T46RCN | | |

3.2.3. Google Earth Engine functions in terms of water indices calculations

3.2.3.1. MNDWI (Modified Normalized Difference Water Index)

Using the characteristics of high absorbability of water and greater radiation of built-up features situated near the river in the short wave infra-red band the limitation of NDWI can be eradicated by constructing a modified version of the NDWI index which is able to differentiate between built-up and water features keeping all the other characteristics of NDWI same (Du et al., 2016). Equation of MNDWI can be written as-

$$MNDWI = (Green - ShortWaveInfrared1)/(Green + ShortWaveInfrared1).....(4)$$

Sentinel-2 band of SWIR wavelength (1610-1613 nm), band11 is used here along with green band, band-3.

But the resolution of band-11 is 20 meters while the resolution of band-3 is 10 meters. This restricted the computation of this spectral index by direct GEE algorithm of band specification.

3.2.3.2. SAVI (Soil Adjusted Vegetation Index)

It is a modified version of another index Normalized difference vegetation index (NDVI) where soil background of vegetation effects of indices are minimized by incorporating a constant soil adjustment factor L. Typical value of L is used as 0.5 (Rondeaux, Steven, & Baret, 1996). Equation of SAVI index is given below-

$$SAVI = \frac{NIR - RED}{NIR + RED} (1 + L) \dots\dots\dots (5)$$

In Landsat 8 surface reflectance products NIR (Near infra-red) region is named as band 5 and specifies the range of wavelength (0.851-0.879 micro meters) and red region is named as band 4 specifies the range of wavelength (0.636-0.673) micro meters.

3.2.3.3. Scale and Google Earth Engine

Using mathematical operations of GEE to calculate MNDWI. But it was found that some part of the study area got misleading values of NDWI. The reflectance pattern of built-up land in the green band and NIR band is similar with that of water, i.e. they both reflect green light more than they reflect near infrared light. As a result, the computation of the NDWI also produces a positive value for built-up land just as for water (Huang et al., 2018).

To calculate the MNDWI values SWIR band and Green band had to be in same resolution. But their resolution differs. In earth engine there's option for specifying scale for analysis as an argument. Green band data was called at a scale of 10 meters so the analysis can be done at the same resolution level.

Step-1. Selecting specific bands for performing an operation

```
Script-1    var bandx1 = qa6.select('B11');
            var bandx2 = qa6.select('B3');
```

- This code goes into the image q6 and selects the band-11 the short -wave infrared band and the band-3 the green wavelength region band

Step-2. Bringing the resolution of band-11 (20 meters) to the resolution of band-3 (10 meters)

```
Script-2    var image_101a = bandx1.resample('bilinear').reproject({
                crs: bandx2.projection().crs(),
                scale: 10
            });
```

- bandx2.projection().crs() selects the projection and crs parameter hidden inside band-3.
- Then it specifies the scale of resampling the pixel values at 10 meters from 20 meters scale.
- Finally using the bilinear resampling method, the output is band-11-pixel values being resampled the values are shown at a pixel resolution of 10 meters in the code editor.

3.2.4. Thresholding of MNDWI in Google Earth Engine in terms of producing informative datasets

3.2.4.1. Normal distributional thresholding

Pixel intensities in an image vary with the brightness values variation. Based on the reflectance characteristics of water MNDWI values usually show values greater than 0 in an image for water (Huang et al., 2018). Objective of this research is associated with finding out the dynamics of water part that's why MNDWI was used as an indicator for water detection hence a threshold of (>0) was used in this regard. Occurrence of pixel values starting from a minimum value to maximum value with a peak in the middle can be distinguished as a distinct feature occurring inside an image if their representative intensities are similar. This phenomenon is known as normal distribution. Histograms are a graphical representation of this distribution (Resources, n.d.). Thresholding of these distributions with this presumption that sufficient number of samples and iterations have been done within the threshold region to achieve the normal distribution can establish a region of real world distinctness relate to the image features (Gervasi et al., 2018). Short difference normal distributions extraction can be very informative in terms of diversity of image features.

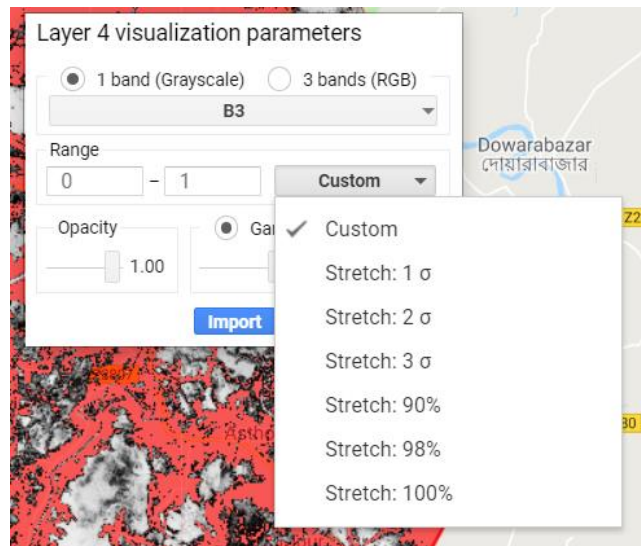


Figure 6 Layer visualization tool in GEE

3.2.4.2. Script by script explanation of steps being followed to threshold the MNDWI values

Step-1. Detection of pixels greater than zero

Applying a threshold of 'greater than zero' using the Boolean operators of google earth engine on the contrast and γ adjusted MNDWI image to detect water. γ and contrast stretch value was set according to the best separation of different levels of brightness occurring inside an image.

Script-1 `Var deepblue4 = (mndwidecember1203 .gt (0))`

Output- Here, mndwidecember1203 is the MNDWI calculated image derived from 03/12/17 Sentinel-2 TOA reflectance image. Greater than zero values occurring pixels are chosen from the image.

Step-2. Masking

Masking the pixels greater than zero from the image.

Script-2 `Var water = mndwidecember1203.mask(deepblue4)`

Outputs- This provided an image with pixels greater than zero value and left other pixels as transparent.

Step-3. Visualization by mapping

Visualizing the map and detecting criteria for choosing areas of sample polygons for histogram representation

Script-3 `Map.addLayer (wet, {min:0, max: 1});`

Outputs- This provided the visualization of the wet image derived from thresholding in the code editor visualization section. Value stretching was mentioned as from 0 to 1, as the threshold was done for values greater than zero, further enhancement of the image was controlled through layer visualization parameters as mentioned before. After several adjustments of these parameters' optimal differentiation of different brightness levels were achieved.

Step-4 Histogram representation

Taking sample polygons over the study area to check for normal distribution of different ranges of values

By visually inspecting the threshold image it was noted there are four levels of brightness inside the image. Google Earth Engine histogram generation script has a limitation of using a limited number of pixels for histogram generation (1000000). That's why specific areas of sample polygon choice were needed to be done based on a specific criterion as histogram generation for the whole image was not possible which would be more suitable.

There were four levels of brightness occurring in the image very bright pixels, medium bright pixels, medium to low bright pixels then leading to totally black pixels showing a variation of values from very high value to low value covering almost all types of brightness variation occurring inside the image. So, the image was divided into above mentioned regions and as much pixels as possible were taken together from these regions to detect at what intervals different normal distributions were occurring.

Script-4

```
var options = {  
  title: 'wet pixels',  
  fontSize: 20,  
  hAxis: {title: 'MNDWI'},  
  vAxis: {title: 'count of MNDWI'}  
}  
  
var histogram1 = ui.Chart.image.histogram( wet ,geometry2,10)  
.setOptions(options);  
print (histogram1)
```

Outputs- The first line is to set the title of the chart as 'wet pixel'.

- The second line sets the font size of the chart as 20 pixels size.
- Horizontal axis name of the graphical representation was set as 'MNDWI'.
- Vertical axis of the graphical representation of the representation was set as 'Count of MNDWI'.
- Histogram over the whole image 'wet' was generated by taking polygons over different regions specified by 'geometry2' and the pixel scale set as 10, so that histograms are generated at native

resolution of the image. Because in Google Earth Engine with each level of zoom level values get resampled. So, specifying the scale of calculation is necessary according to the image resolution.

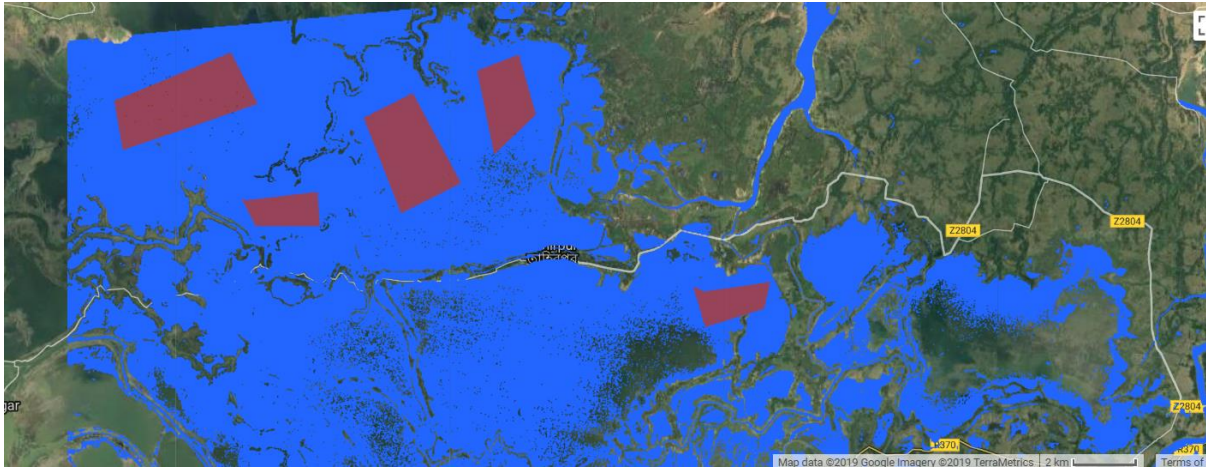


Figure 7 Sample polygons taken over a homogenous region to detect normal distribution

The histogram below is generated from the polygons taken over the whole study area shown in figure-8. The red circles denote starting of each normal distribution. This was detected by each time a distribution of pixel values occurrence minimum to maximum with a peak of value occurrence in the middle. Whenever after the previous minimum value a higher value of occurrence was detected that was taken as the starting range of the next normal distribution. Optimum value for distinct normal distribution was selected by manipulating these values iteratively for each of the ranges, by increasing number of sample polygons for each iteration and by comparing with high resolution imagery to check for homogenous area covered by the threshold. For Soil Adjusted Vegetation Index (SAVI) values also same procedure was followed. Normal distribution was found in three levels of ranges high range, medium range and low range. The values of ranges and corresponding covering areas are provided in the results section along with MNDWI values.

Usage of the literature derived values (section 2.2) as particular features occurring inside an image can give furthermore information and naming of such features occurring inside an image. Besides, integrating these assumptions with the similarity of comparison with high resolution imagery was done to ensure the distinction of ranges.

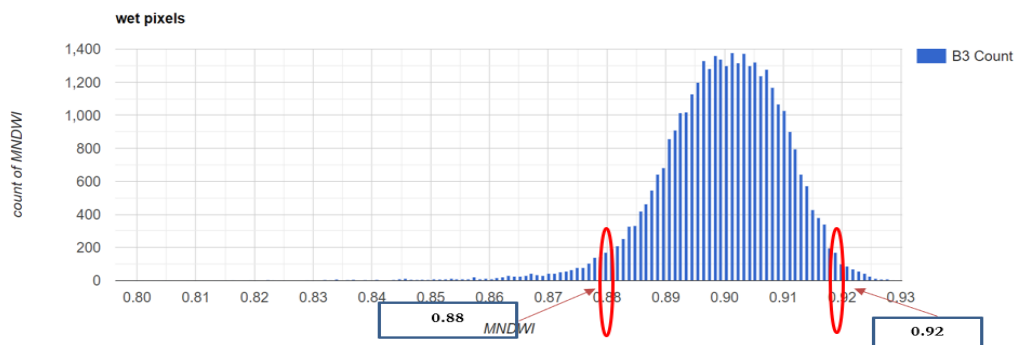


Figure 8 polygons generated normal distribution

When the normal distribution ranges didn't match the literature-derived values directly, we relied on visual interpretation from high resolution images for that part. Also, while within the literature derived a mixture of more than one normal distribution range was found, the same approach of comparison with high resolution imagery supported to distinguish the sections.

3.2.5. Reclassification

3.2.5.1. Merging of similar characteristics indicative separate distributions into one common class by reclassification of thresholding ranges

Reclassification merging of normal distributions for water cover dynamics- 1. (highly turbid, medium turbid and less turbid) to water and 2. (Soil with high water content and waterlogged areas of vegetation) to either wet soil or waterlogged i.e. moist soil to simplify the calculation of integration for summing up these images to look at the water and vegetation dynamics. Besides, as our objective is to look at the hydrologic and vegetation regime dynamics as mentioned earlier, narrow range separation of classes is not needed in this case. Normal distribution of narrow ranges helped to clarify the water covered areas at smaller scale which increased the probability of avoiding erroneous result for separation of water regime.

SAVI index is a measure of crop growth or presence of vegetation cover (Xue & Su, 2017). Vegetation cover can be defined as the percentage of an area covered by vegetation. Hence, dynamics of vegetation from the context of SAVI index here can be quantified as areas containing low percentage of vegetation cover turning into areas containing high percentage of vegetation cover (Xue & Su, 2017). That's why the normal distribution ranges of SAVI index which also corresponded with different levels of vegetation cover occurring in the study area while being compared with the ground truth i.e. high-resolution images of the study area has not been merged into further summation of ranges, mere attribution of different classes was carried out.

3.2.5.2. Script by script explanation of MNDWI and SAVI thresholding steps

Step-1. Creating a constant value image

There's no any direct function provided in Google Earth Engine to reclassify a range of values into one single class by assigning an attribute to this range. Hence, to replace a range by a single value which would work as the attribute value of that specific class a constant value image was created as in Google Earth Engine most of the functions and outputs are image-based or map-based.

Script-1 **Var image1 = ee.Image(1)**

Output- Creates an image where each pixel contains a value of 1. Another 2 images were also created with values of 2 and 3 according to the requirement of ranges to be replace occurring inside an image, these images were used.

Step-2. Replacing range of values using the integer values from constant images

For replacing the normal distribution ranges constant images were used to replace the ranges by an integer to which can work as the representative of a specific class.

Script-2 **var reclasswater = (water1617.where((water1617.gt(0.6)).or(water1617.eq(0.6)), image1))**

Output- This function goes to the 'water1617' image which is the mask result of MNDWI values greater than 0.6 or equals to 0.6 and through the 'where' function it goes to the specific pixel locations of that image and replace those pixels with constant value of 1. This way this segment of normal distribution turns into a single image specifying a class. In this case it is water. When merging of classes was done, we simply change the range inside the script according to our requirements here in this case, highly turbid areas were found

as ranges of greater than or equals to 0.930 and less turbid areas as smaller than 0.930 and greater than or equals to 0.6. As we decided to merge the different turbidity distinctions in one class of water the range value was specified as greater than 0.6 or equals to 0.6. For each date image this reclassification was done repetitively. For water dynamic-ranges of waterlogged areas were also merged with the soil with high water content class ranges and the whole class was attributed as soil with high water content and the values of this range was replaced by 2. And the non-water part was attributed as 3. Each image was attributed separately but into 3 common classes as mentioned.

SAVI values were attributed as 1, 2 and 3 for high percentage of vegetation cover, medium percentage of vegetation cover and low percentage of vegetation cover.

Step-3 Mosaicking the reclassified images

Mosaicking refers to the process of spatially assembling image datasets to produce a spatially continuous image. Every range resulted in a sperate masked image. Reclassification was done inside those masked ranges. By mosaicking they were merged together to get back its original extent.

Script-3 `var novemberreclassified1617a = ee.ImageCollection ([water1617, waterloggedvegnovmask1617,nonwatermask1617]).mosaic()`

Output- The 'ee.ImageCollection' function creates a stack of reclassified images here of same date here the image is of 3rd November and joins together different locations covered by different reclassified images. Here, the water1617 covers the water part, waterloggedvegnovmask1617 covers the wet soil part and nonwatermask1617 covers the part of soil with low water content throughout the study area resulting in a classified image of that day. This way for each day reclassified images of MNDWI and SAVI were joined together and classified images for the available images within that period were derived.

3.2.5.3. Script by script explanation of using aggregate functions

Compositing refers to the process of combining spatially overlapping images into one single image based on different types of aggregation functions. Aggregation functions can be defined as process of summarizing values depending on different arithmetic functions. This facilitates utilization of aggregation functions according to the requirements of deriving appropriate classes based on their dynamic characteristics. This helps to relate the wetland with larger landscapes and places considerations of the wetland dynamic characteristics from different aspects from any broader context as landscapes or watersheds etc (Sutter, 2014). According to the section 3.3.2.3 to understand the dynamics of water, identification of permanent water body, permanently non-water and areas of transitional water body occurring within a wetland is necessary.

1. Detecting areas of permanent inundation and non-inundated areas

Script-1:

```
var permanentwater = ee.ImageCollection ([novemberreclassified1617,
novemberreclassified1617a,decemberreclassified1617b,reclassifiedjanuary1617e,febreclasswater1617f]).max()
```

Script-2:

```
var permanent non-water = ee.ImageCollection ([novemberreclassified1617,
novemberreclassifies1617a,decemberreclassified1617b,reclassifiedjanuary1617e,febreclasswater1617f]).min()
```

Output- In this image collection inputs are the reclassified images of MNDWI. All the attributes inside the brackets are variable names of images. Each image has three attributes water, soil with high water content and soil with low water content i.e. non- water which are represented by integer values of 1, 2 and 3 inside the image. This function maximum goes through each image inside the image collection and finds out the maximum value occurring inside that pixel over all the images specified in the bracket sequentially. Hence in the output the pixel is provided with the maximum value occurring inside that pixel over all the spatially overlapping images. Hence, the pixels where in the output the value is 1 that means in that pixel no value greater than 1 has been occurred within the images present in the collection. Hence these locations that are 1 in the output image has always been water within this post to pre-monsoon period in 2016-17 year meaning these areas are permanent water body for that period. In this method permanently inundated areas of year 2017-18 also permanent areas of low soil moisture and through SAVI index permanent areas of high percentage of vegetation cover and areas of low percentage of vegetation cover was found out. Output maps of this section are provided in the results section.

To detect the areas of non-inundated permanent areas the same method was applied by applying minimum function this time. In this method the function goes into the image collection in each image of each pixel and finds out the minimum value occurring in that pixel. The low soil moisture areas in each image in the collection is attributed as 3 which is the highest value occurring among all the attribute values. Hence, in the output in the pixels where this value is occurring is the minimum value hence no value less than that value occurred in that pixel which is the highest value of the image. Hence in these pixels no value less than 3 ever occurred among all the images which classify these areas of non-inundated areas. The same way the areas which always show high percentage cover of vegetation and low percentage cover of vegetation were identified.

2. Integrating the results of aggregation function with the daily results of MNDWI and SAVI indicated locations to predict about the locations of transitory water parts

Permanent water and non-water parts of the study area are those parts where the cover didn't change over the whole study period over two years of 2016-17 and 2017-18. Hence if somehow these areas could be separated from the daily images of the MNDWI and SAVI images dynamics of transitory water bodies over the whole study period could be understood and the dominant covers occurring each month and the conversion of their transition process over time could also be understood from both water dynamics and vegetation dynamics point of view. To separate these areas and derive the transitional parts following scripts were sequentially followed-

Script-1.

```
var x = (permanentwater.neq(1)).and(nonpermanentwater.neq(3))
var transitorynov = novemberreclassified1617.mask(x)
var transitoryveg1 = reclassifiedvegnovember1617e.mask(x)
```

Output: The first script chooses the pixels that are not equals to 1 from the permanent water body and non-permanent water body images where permanent water body is attributed as 1 and permanent areas of non-permanent water body is attributed as 3 from respective images and creates a mask which now contains all the pixel locations inside those two images except the permanent and permanent non- water bodies. The second and third script just uses this mask to derive the locations of these pixels in the daily reclassified maps. This basically provides us with all other areas except the overtime constant permanent water and areas of low soil moisture i.e. non-water areas. This is not a pure estimation of transitory water parts as there may be soils with high water present in this masked part which don't get flooded. But from image by image masking of every MNDWI image these areas can be identified by comparing with each other. The same way if we mask out every SAVI image, we will find also the percentages of vegetation covers occurring in this transitory part.

3.2.6. Exporting images to QGIS

In Google Earth Engine when images are composited together based on an aggregation function permanent water features are identified from the output based on their values of pixel accumulation. But besides the permanent feature indicating value or any other desired value there are other values occurring inside the image. To separate the desired portion of analysis there are Boolean functions provided in Google Earth Engine. But these functions work as masks hence the desired output contains masked pixels which need to be unmasked to perform further calculations with the output. When unmasking is done along with the desired output this unmask the whole code editor pixels which is undesirable for further visualization of the maps. To proceed with the change calculation with the derived permanent waterbody, transitory waterbody and percentage of vegetation cover maps hence these maps were further exported to QGIS software.

1. Change between 2016-17 permanent waterbody to 2017-18 permanent waterbody was calculated by image subtracting in QGIS as-

$$(2017 - 18) \text{ permanent water body} - (2016 - 17) \text{ permanent water body} \dots \dots \dots \dots \dots \dots 6)$$

2. Change between 2016-17 drier soil areas and 2017-18 drier soil areas were calculated by image subtracting In QGIS as-

$$(2017 - 18) \text{drier areas} - (2016 - 17) \text{drier areas} \dots \dots \dots (7)$$

3. Change between 2016-17 Permanent areas of high percentage of vegetation cover and 2017-18 permanent areas of high percentage of vegetation cover areas were calculated by image subtracting in QGIS as-

$$(2017 - 18) \text{high percentage of vegetation cover} - (2016 - 17) \text{high percentage of vegetation cover} \dots \dots \dots (8)$$

4. Change between 2016-17 low percentage of vegetation cover areas and 2017-18 low percentage of vegetation cover areas were calculated as-

$$(2017 - 18) \text{low percentage of vegetation cover} - (2016 - 17) \text{low percentage of vegetation cover} \dots \dots \dots (9)$$

3.2.6.1. Calculation of land cover conversion of transitory parts

To calculate the land cover conversion within transitory water parts the masked images derived from section 3.3.2.5 part-2 script-2, were exported in QGIS. Then each image classes were attributed as

- Water = 1
- Soil mixed with moisture = 2 and,
- Drier soil = 4

Then, every two months difference was calculated to get the dynamics in a two months interval-

- 1. January map – November map**
- 2. March map – January map**

The values were interpreted as-

- 1-1=0, no change
- 2-2=0, no change
- 3-3=0, no change
- 1-2=-1, soil mixed with moisture to water
- 2-1=1, water to soil mixed with moisture
- 4-2=2, soil mixed with moisture to drier soil
- 2-4=-2, Drier soil to soil mixed with moisture
- 1-4=-3, Drier soil to water
- 4-1=3, Water to drier soil

3.2.6.2. Calculation of changed areas

For each change map the amount of area of change whether area increased or decreased was calculated by multiplying the number of pixels covered by each class by the cell size of pixels.

$$\text{Areas of change} = \text{cell size} * \text{Number of pixels in each class} \dots \dots \dots (10)$$

To calculate the percentage of areas covered by each conversion of land cover type from month to month mentioned in section 3.3.2.7, areas of each conversion was calculated using equation (10), then each areas were divided by the area of the whole study area and multiplied by 100 to get the percentage of conversion type coverage-

$$\begin{aligned}
 & \text{percentage of area covered by each conversion type} \\
 & = \frac{(\text{cell size} * \text{number of pixels covered by each conversion type})}{(\text{Total area of the study area})} \\
 & * 100 \dots \dots \dots (11)
 \end{aligned}$$

3.2.7. Exporting images to ILWIS

Images from the year 2016-17 were exported in ILWIS to sum up the maps through creating a map list of these images and then calculating map list statistics as sum of all these images to delineate different degree of susceptibilities of specific locations over the hydrologic regime of the study area to specific types of dynamics. To do this, every image was attributed as water =1, moist soil =5 and dry soil =21. These values were chosen so that the possibility of occurring the highest value in the output sum image for a certain feature always stays lower than the immediate next feature occurring this way permanency of the respective features in one image can be detected as highest values will not be corrupted with other features value mixtures. But this has a problem of interpreting other conditions such as intermediate values. But comparing the quantity of the output image pixel values and the number of images used in analysis these values can also be interpreted as number of times one particular feature occurring. The classification was done in the following way-

Value with 4 is permanent water (1+1+1+1), less than 4 value was 3.30 to 3.60 which is nearable to permanent (1+1+1+0.6 or either way) no value occurred. This shows every month these pixels had water.

Values from 5-20 was classified as- 5 being only once moist soil occurred there other times it was water. Hence, water areas which can turn into soil at certain times but very rarely.

10 being soil occurring two times over these four months hence has a higher susceptibility to turn into soil, 15 more than previous and so on. 20 is the value of permanent areas which are always moist soil. As (5+5+5+5) = 20 meaning each month moist soil is occurring there. Same way dry soil areas were also classified.

4. RESULTS

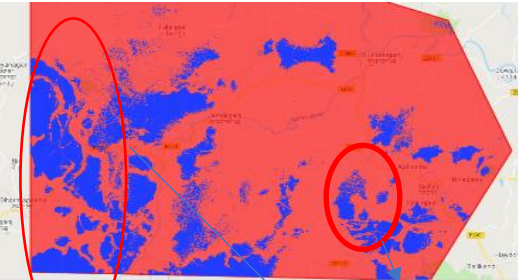



After several iterations and comparison different range of values occurring in the image showed a homogenous and normal distribution that is compared with high resolution images to compare with the visual trueness of homogeneity of normal distributional distinction as much as possible.

4.1. Overview of Planet high resolution images used for comparison with thresholded image

Planet operates the largest constellation of Earth-imaging satellites ever. It offers a diverse selection of medium and high-resolution data products under one roof. By accounting for the effects of the atmosphere, sensor characteristics, and incident solar radiation, Planet provides as near as possible to true reflectance of the Earth's surface. These images are provided in the planet platform as true colour visible band combination images with 3 meters resolution and projected in UTM projection. All planet data are from Planet Team (2018). *Planet Application Program Interface: In Space for Life on Earth*. San Francisco, CA. <https://api.planet.com>.

4.2. Normal distribution results from November 2017 and comparisons with high resolution image

Table 2 : Procedure of selecting normal distribution

| Image date | Range-1 | Range-2 |
|------------|---|--|
| 2017-11-03 | (>.930) | (<0.930 and >0.6) |
| |  |  |
| |  |  |

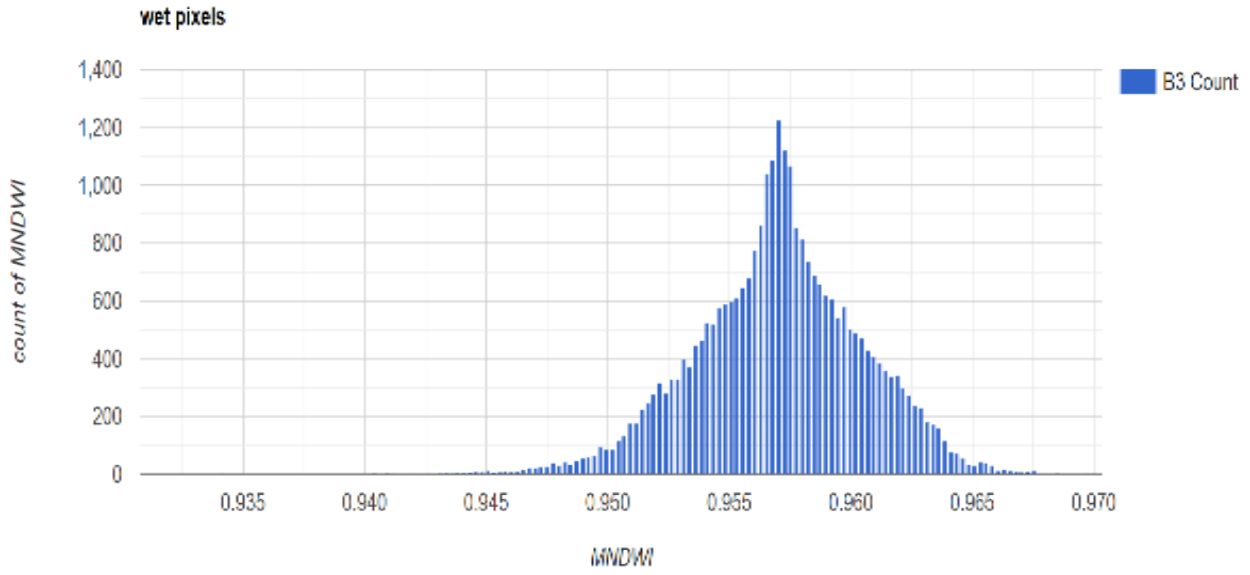


Figure 10: Normal distribution for >0.930

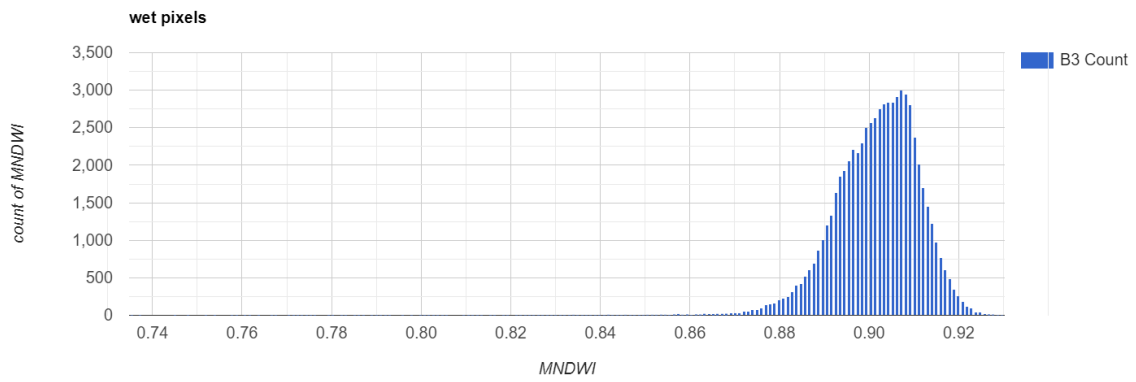


Figure 9: Normal distribution range for <0.930 and >0.6

4.3. Overview of month to month temporal dynamics of hydrological regime MNDWI thresholds and vegetation regime by SAVI thresholds

Results from 2017 November to 2018 March normal distribution ranges covering areas are put together in a table (There are more than one images were found in each month and being used in our analysis. In this section one image from starting month of post monsoon-November, one image from January and one image from March is represented to indicate the overall dynamics of this post-monsoon to pre-monsoon time period hydrological and vegetation conditions behaviour)

Table 3 Thresholds for November 3rd image


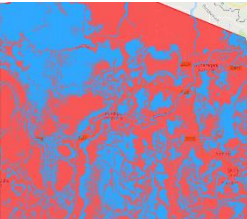
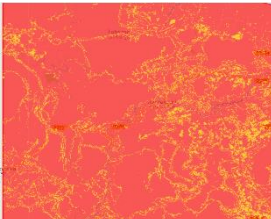
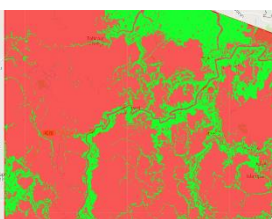
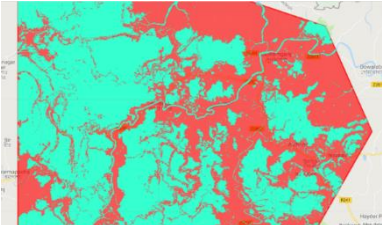
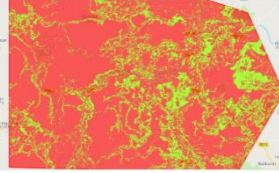
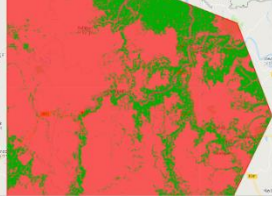
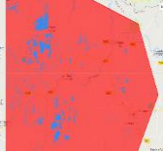

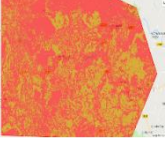
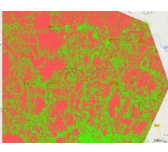
| Image date | <p>MNDWI (areas delineated by deep blue color with a threshold range of >0.930 MNDWI value) (Named as highly turbid according to 2.2 literature review derived MNDWI values and section 4.2 procedure)</p> | <p>MNDWI (areas delineated by cyan blue color with a threshold range of <0.930 and >0.6 MNDWI value) (Named as Less turbid according to 2.2 literature review derived MNDWI values and section 4.2 procedure)</p> | <p>MNDWI (areas delineated by cyan yellow brownish color with a threshold range of <0.6 and $(>-0.1$ or eq $-0.1)$) (Named as Wet soil and shallow water with waterlogged vegetation according to figure 2 of 2.2 literature review and section 4.2 procedure)</p> | <p>MNDWI (areas delineated by green color with a threshold range of <-0.1 MNDWI value) (Named as Soil with low water content according to figure 2 of 2.2 literature review and section 4.2 procedure)</p> |
|------------|---|--|--|---|
| 2017-11-03 |  |  |  |  |
| | <p>SAVI (areas delineated by deep cyan blue color with a threshold range of $lt -0.1$ index value) (Named as low percentage of vegetation cover according to (Rondeaux et al., 1996) and section 4.2 procedure)</p>  | | <p>SAVI (areas delineated by yellowish green color with a threshold range of Less than 0.1 and (greater than or equals to -0.1 index value) (Named as medium percentage of vegetation cover according to (Rondeaux et al., 1996) and section 4.2 procedure)</p>  | <p>SAVI (areas delineated by deep green color with a threshold range of $(>0.1$ or eq $0.1)$) (Named as low percentage of vegetation cover according to (Rondeaux et al., 1996) and section 4.2 procedure)</p>  |

Table 4: **Thresholds for January 22nd image**

| | | | | | | |
|----------------------------------|---|--|---|--|---|--|
| <p>201 8- 01- 22</p> | <p>MNDWI (areas delineated by deep blue color with a threshold range of >.745 MNDWI value) (Named as highly turbid according to 2.2 literature review derived MNDWI values and section 4.2 procedure)</p> | <p>MNDWI (areas delineated by lighter blue <0.745 and >0.71 or eq 0.71) (Medium turbid according to 2.2 literature review derived MNDWI values and section 4.2 procedure)</p> | <p>MNDWI (areas delineated by cyan blue with a threshold <0.71 and >0.61 or eq 0.61) (Less turbid) (Less turbid according to 2.2 literature review derived MNDWI values and section 4.2 procedure)</p> | <p>MNDWI (areas delineated by yellow brownish with a threshold <0.61 and >0.2 or eq 0.2) (named as Water-logged vegetation according to 2.2 literature review derived MNDWI values and section 4.2 procedure)</p> | <p>MNDWI (areas delineated by light green <0.2 and >-0.1 or eq -0.1) (named as Soil with high water content according to 2.2 literature review derived MNDWI values and section 4.2 procedure)</p> | <p>MNDWI (areas delineated by deep green <-0.1) (named as Soil with low water content according to 2.2 literature review derived MNDWI values and section 4.2 procedure)</p> |
| |  |  |  |  |  |  |


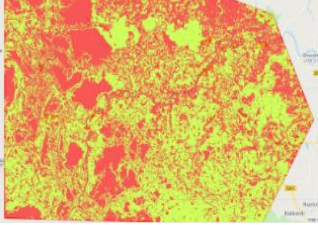

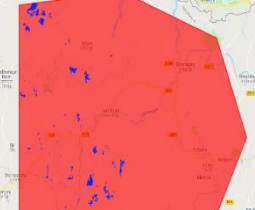
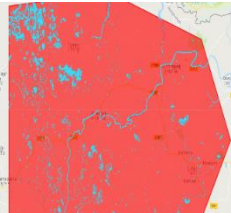
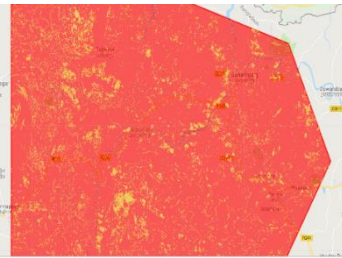

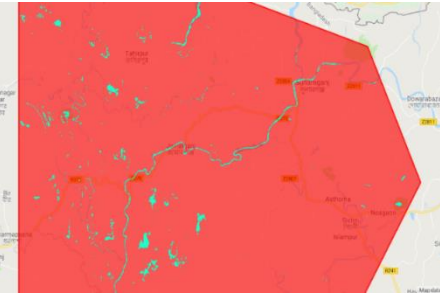

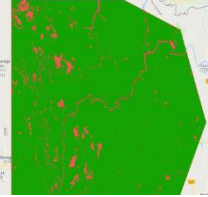
| | | | |
|--|---|---|---|
| | <p>SAVI lt (0) Low percentage of vegetation cover areas delineated by deep cyan blue color with a threshold range of lt 0 index value (Named as low percentage of vegetation cover according to (Rondeaux et al., 1996) and section 4.2 procedure)</p>  | <p>(SAVI < or equals 0.13) and (> or equals 0) (Medium percentage of vegetation cover areas delineated by deep cyan blue color with a threshold range of less than or equal 0.13 and greater than or equals 0 index value)</p>  <p>(Named as medium percentage of vegetation cover according to (Rondeaux et al., 1996) and section 4.2 procedure)</p> | <p>SAVI (gt 0.13) (Named as high percentage of vegetation cover according to (Rondeaux et al., 1996) and section 4.2 procedure)</p>  <p>delineated by deep green color with)</p> |
|--|---|---|---|

Table 5: Thresholds for March 23rd image

| | | | | |
|-------------------|--|--|---|---|
| <p>2018-03-23</p> | <p>MNDWI (>0.74) (Highly turbid) (Same procedure followed)</p>  | <p>MNDWI (<0.74) and (>0.3 or eq 0.3) (Less turbid) (Same procedure followed)</p>  | <p>MNDWI (<0.3) and (>-0.1 or eq -0.1) (Soil with high water content) (Same procedure followed)</p>  | <p>MNDWI Lt (-0.1) Soil with low water content (Same procedure followed)</p>  |
| | <p>SAVI (lt 0) Very low density of vegetation</p>  | <p>SAVI (gt or eq 0 and lt 4 or eq 4) Medium density of vegetation</p>  | <p>SAVI (gt 4) High density of vegetation</p>  | |

4.4. Hydrological and vegetation dynamics explained from above table through thresholding of spectral indices

The first two MNDWI normal distribution range in table-3 are identified as turbid images which encompass the total watery part of the study area during 2017-11-03. Just after the normal distribution indicator range of turbid areas, there is another normal distribution occurring wet soil or shallow water with waterlogged vegetation showing a less range of MNDWI values as we know for gradual emergence of soil/decreasing depth the SWIR reflectance also gradually increases and MNDWI range value also tend to decrease. The negative range of MNDWI hence identified as non-water (Singh et al., 2014). SAVI ranges of low percentage of vegetation cover complements the watery area locations detected for that day. The areas of low percentage of vegetation cover are the summation of highly turbid and less turbid areas identified by MNDWI images in the table. Non-water areas are also complemented by presence of high density of vegetation. Areas of shallow water with waterlogged vegetation or that may be wet soil as it is hard to distinguish between these two by mere measurements of MNDWI values, SAVI shows in these locations medium amount of density of vegetation presence. As the segmentation of SAVI values were done also the same way by finding normal distribution of each section and high range of section usually indicate presence of high density of vegetation (Xue & Su, 2017), this medium range was indicating a normal distribution in between high range of values and low range of values. As vegetation coverage and presence of water content on that soil are negatively correlated hence these two images also complement each other according to their conditions (Xue & Su, 2017)

January 22nd image in table-4 shows a dry period image which indicates as seasons are creeping towards from post monsoon to pre-monsoon the ranges of corresponding segments are decreasing i.e. MNDWI values are decreasing meaning emergence of soil in those areas is gradually accelerating. This is also supported by the emergence of vegetation in those areas which is indicated by the SAVI values. The locations which were characterized as watery area in the November image of 2017, in 2018 January those areas are turning into either water-logged vegetation or into soil with high water content. Another thing to notice is in the November image the water-logged area and the soil with high water contents were mixed with each other so much a distinct normal distribution of MNDWI was hard to be found which is why it couldn't be differentiated between those areas. Now, when the emergence of soil is getting higher more areas with high water content except water-logging conditions are getting emerged or the water is getting soaked up in the areas of water-logged conditions which is paving the way for soil with high water content as a separate condition specific cover occurring in the study area. And these areas are from the SAVI point of view the areas of medium density of vegetation. Non-water areas didn't change that much they almost remained the same both in SAVI and MNDWI identification over this period.

March 23rd MNDWI image in table-5, last image of our analysis period the closest one to the pre-monsoon also which is the last image from the dry period, is actually an image when the weather warms up and soil is being prepared for planting of Boro rice (JICA, 2013). From the previous two images of November and January here we can see the watery part decreased a lot and most of the watery and waterlogged vegetataed covers have changed into soil with low water content areas which are actually vegetated areas may be an indication of Boro rice plantation being started there.

4.5. Results from reclassified MNDWI and SAVI mosaics

The main purpose of reclassification was to give attributes for each class as arithmetic integer values representing a specific range i.e. a class so that by manipulating these values algebraically or through usage of algorithms an overall perception of locations of a class occurrence could be obtained.

Apart from that, as objective of this research is to find out the hydrological dynamics which depends on the understanding of transformation of wetland water state to soil and vice-versa, separating among different turbidity levels or waterlogged and high soil moisture is less important here. Furthermore, for detection of waterlogging situation needs measurement of depths as proof but the thresholds are only dependent on the interpretation of high-resolution images and normal distribution. Soil mixed with water can be more clearly identified from these images as perception of depth by mere visual inspection can be erroneous. Hence, all the areas which were classified as waterlogged situations are merged with soil with high moisture classes and a new name given to this class as soil mixed with water was given to this range. New reclassified images of MNDWI were simplified into three classes-

1. Water (all turbidity merged together)
2. Soil mixed with water (waterlogged and soil with high moisture merged together) and
3. Soil with low moisture.

This also reduces the risk of inaccuracy in derived locations of respective classes after integrating reclassified images.

For SAVI no change of range values was done, simply the ranges were attributed as distinct classes for further procedures as here visual inspection of percentage of vegetation covers and normal distribution corresponded well and created less confusions.

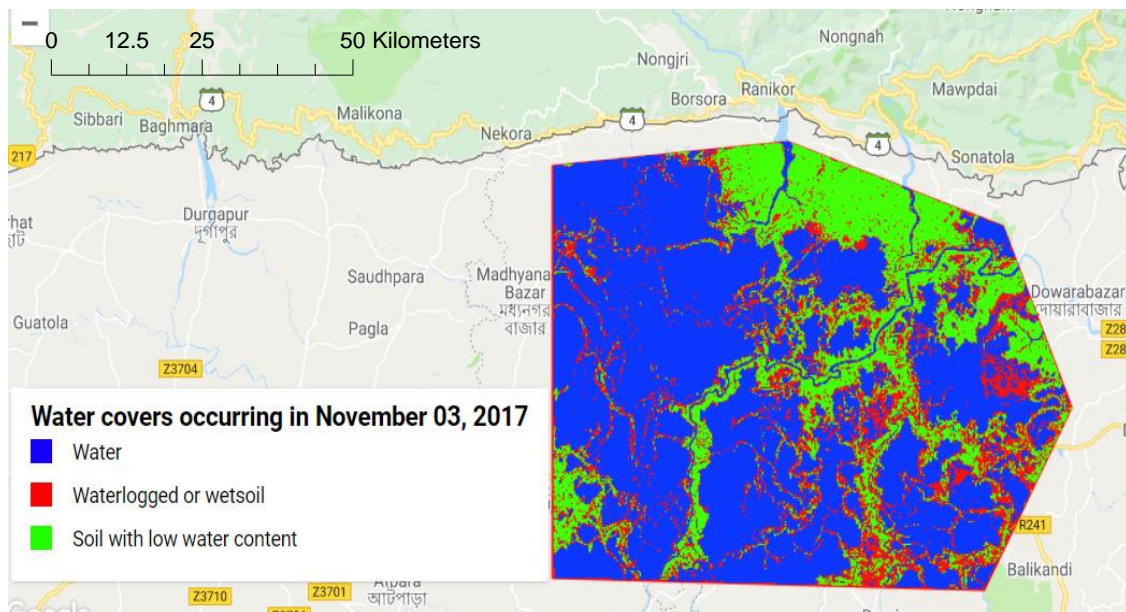


Figure 11 Reclassified image of MNDWI thresholds from November 03, 2017

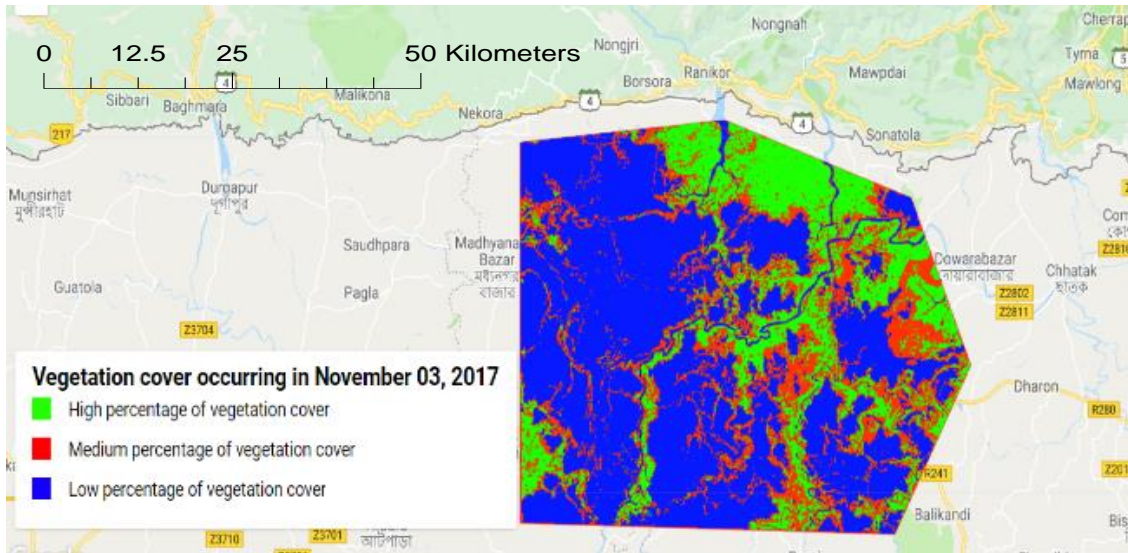


Figure 12 Reclassified SAVI image

4.6. Results from integration of temporal dynamics

4.6.1. Hydrological regime

4.6.1.1. Location and extent of permanent water in Tanguar Haor during post-monsoon to pre monsoon

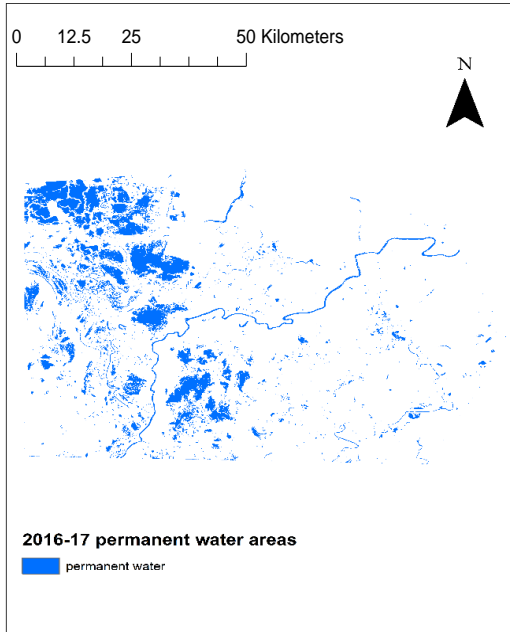


Figure 13: Permanent water bodies of 2017-18

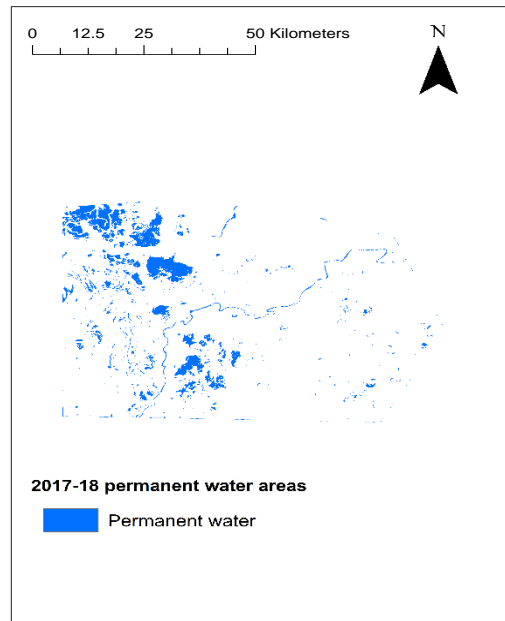


Figure 14: Permanent water areas of 2017-18

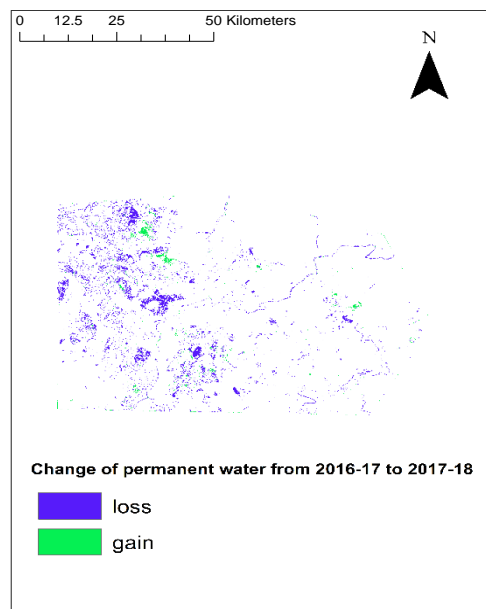


Figure 15: Permanent water bodies that changed from 2016-17 to 2017-18

Here, figure-13 and figure-14 is showing the permanent water extent for 2016-17 and 2017-18 for two years of period during post-monsoon to pre-monsoon season. Figure-15 is the locations showing the changes occurred from 2016-17 to 2017-18. This is basically the result of that image differencing mentioned in the methodology.

4.6.2. Vegetation regime

4.6.2.1. Location and extent of high percentage of vegetation cover in Tanguar Haor during post-monsoon to pre-monsoon season

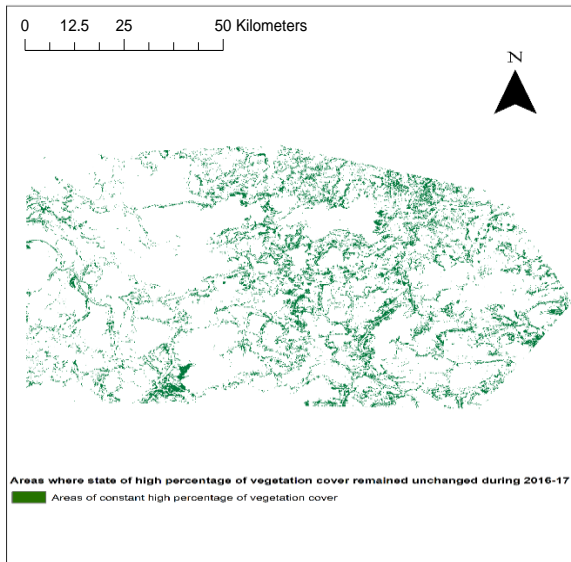


Figure 16: Permanent areas of high vegetation 2016-17

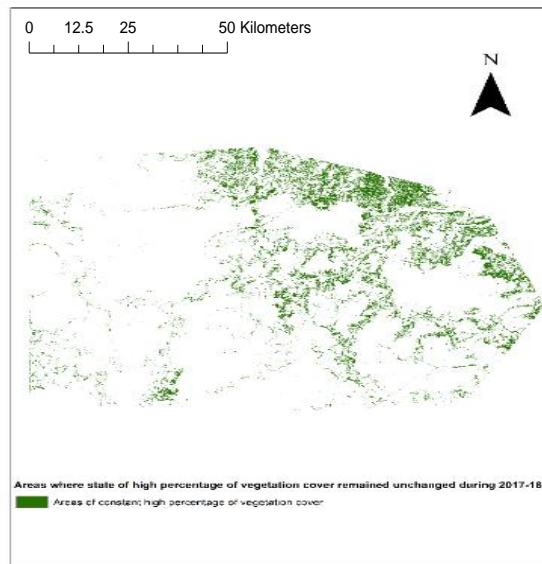


Figure 17: Permanent areas of high vegetation 2017-18

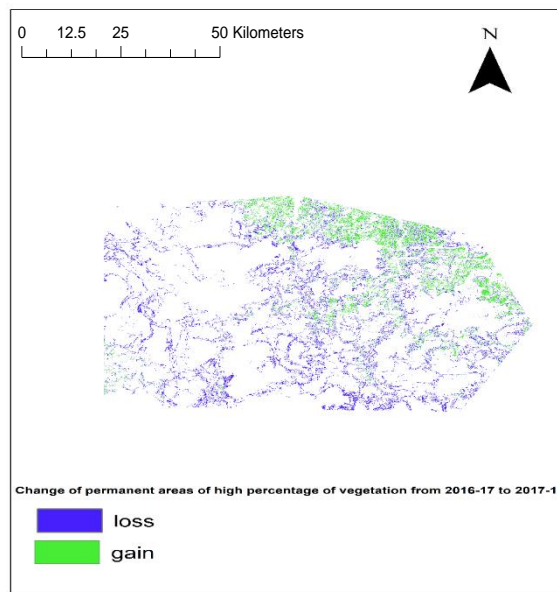


Figure 18: Change of permanent areas of highly vegetated areas from 2016-17 to 2017-18

Figure 16 and figure 17 show the areas where vegetation coverage percentage always stayed in the higher side over the pre monsoon to post monsoon season for 2016-17 and 2017-18 respectively. Figure 18 shows the areas of these permanent vegetation cover change from 2016-17 to 2017-18.

4.7. Results from November to January cover change showing transitory part of water during 2017-18 to understand transformation from one cover to another over time

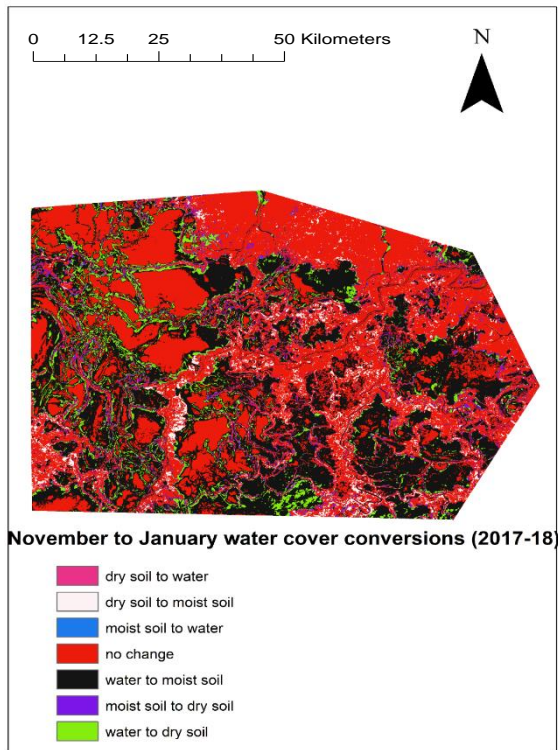


Figure 20: November to January conversion dynamics within post-monsoon to pre-monsoon season delineating transitory parts of Tanguar Haor.

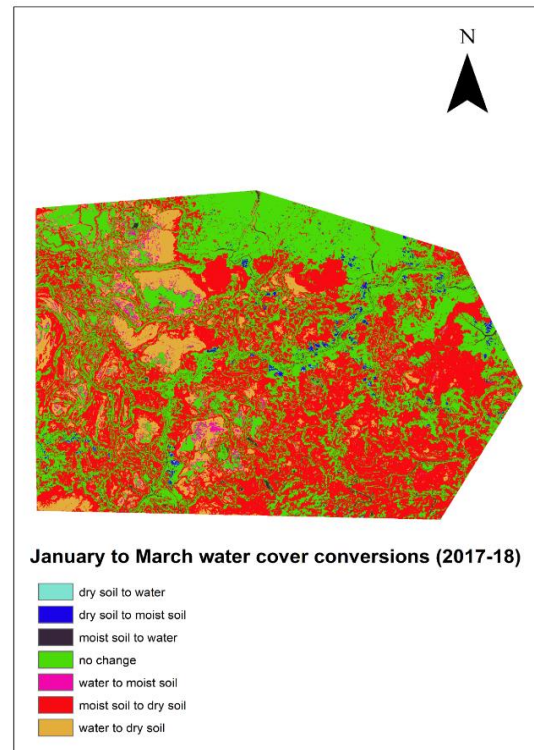


Figure 19: January to March conversion dynamics within post-monsoon to pre-monsoon season delineating further transition from figure-20

Figure-20 shows the areas of dry soil to water, moist soil to water, water to moist soil and water to dry soil which are delineated by white, blue, black and green respectively are the areas of transitory water parts which changed their state from water to another cover or vice-versa during November to January. Figure-19 shows the areas of dry soil to water, moist soil to water, water to moist soil and water to dry soil which are delineated by cyan, black, pink and light orange respectively. Figure 20 transition and figure 19 transition parts together make up the transitory water regime of post monsoon to pre-monsoon period.

4.8. Comparison of areas changed between hydrological regime and vegetation regime throughout pre-monsoon to post-monsoon season from 2016-17 to 2017-18

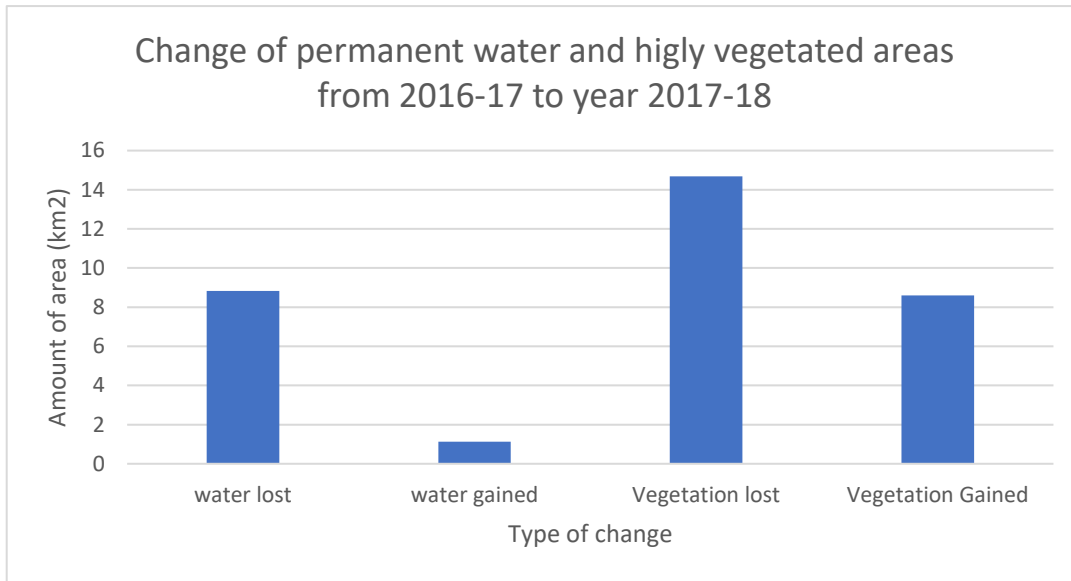


Figure 21: Amount of change in hydrological and vegetation regime area in square kilometers

Figure-21 shows from 2016-17 to 2017-18 post to pre-monsoon season both hydrological and vegetation regime experience a significant amount of water and permanently vegetated area being lost. Comparing to the amount of loss gaining i.e. increase in overall post to pre-monsoon water regime area and vegetated area was very low. In terms of amount of area being covered both in terms of loss and gain the quantity of vegetated area was higher compared to the hydrological regime.

4.9. Comparison of areas coverages by different conversion type for the year 2017-18 from pre-monsoon to post-monsoon season showing transitory water cover conversion

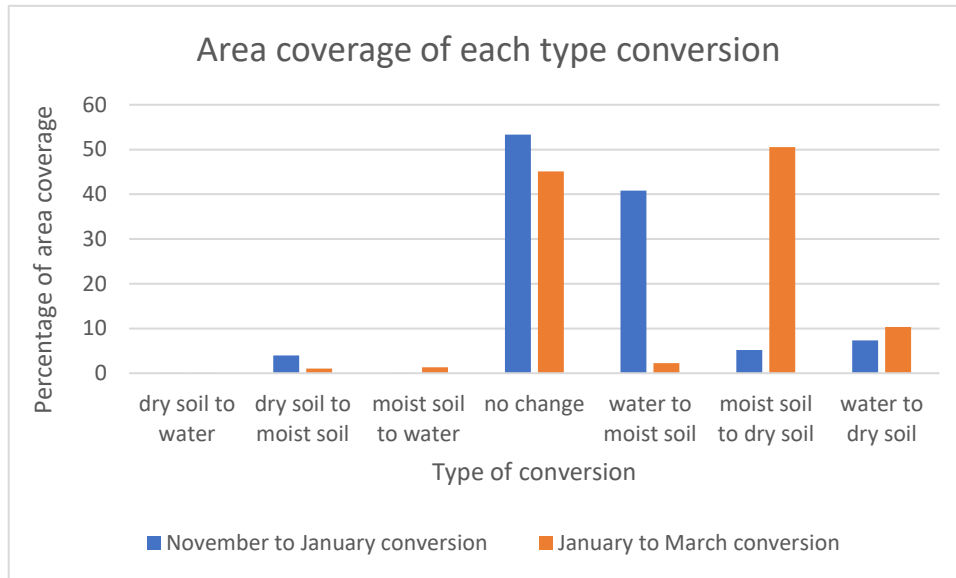


Figure 22 Area coverages of water cover conversions

Transitory water part is the part of wetlands that is subjected to ephemeral flooding from dry condition or any type of liquid-free state of wetland cover (section-2). Figure-21 shows four types of conversion from dry or moist soil condition to the only liquid state of this wetland which is water, can occur. They are-

1. Dry soil to water (November to January - 0% coverage)
(January to March- 0% coverage)
2. Moist soil to water (November to January - 0 % coverage)
(January to March - 3-4%)
3. Water to moist soil (November to January - 40%)
(January to March- 4-5%)
4. Water to dry soil (November to January - 8%)
(January to March – 10%)

This shows the highest transition occurs during November to January which is the post monsoon to dry season period and the type is water turning into moist soil.

Most of the study area is subjected to no change throughout this period. Apart from the transitory part the highest conversion that occurs in the study area (51%) is moist soil being turned into dry soil which is actually the highest among all types regardless of transitory part. This is higher than even the water to moist soil. As the source of moist soil which is becoming drier is the saturated soil of November to January this shouldn't be higher than the water to moist conversion coverage of the study area. The reason of this increase in coverage is some parts of moist soil was also turning into dry state during November to January. Besides, water also turning into moist soil in January to March period and simultaneous conversion was happening during that period which increased the coverage of moist soil turning into dry soil.

4.10. Map showing locations of different levels of susceptibility to water dynamics all derived together in one image

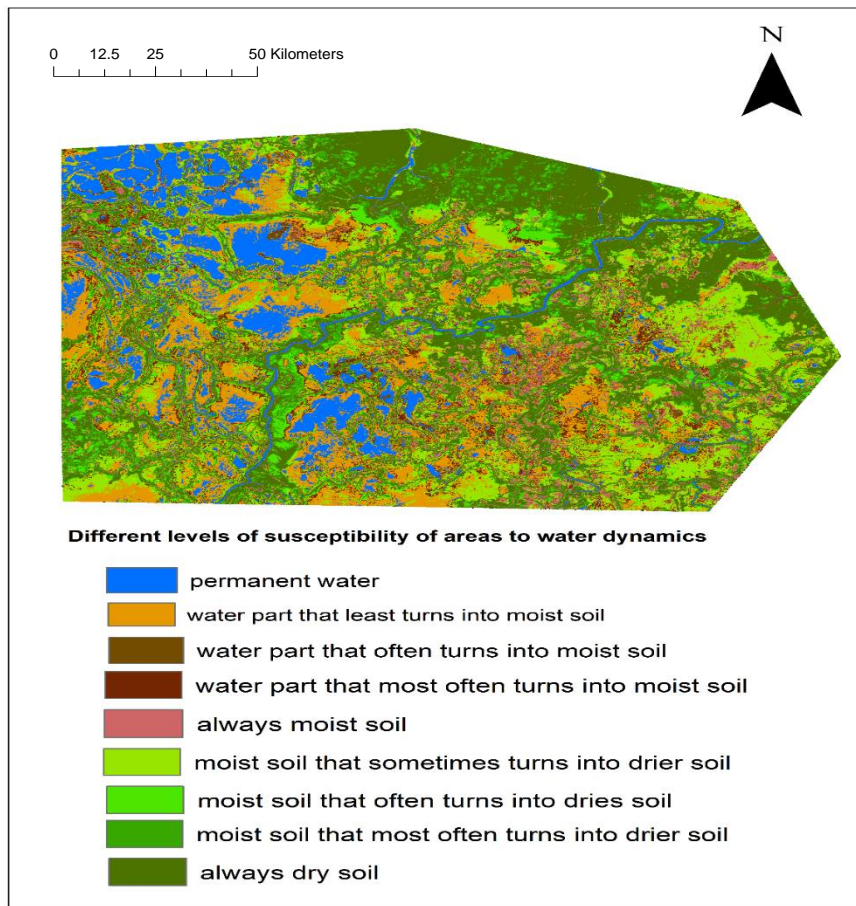


Figure 23 Frequency of different conversion processes occurring throughout the study area.

This frequency map contains specific places throughout the study area depicting the number of times each conversion process is happening there. The main two conversion process that happens here are

Brown- water part that least turns into moist soil

Light green- Moist soil that sometimes turns into drier soil

This map hence is an extended interpretation of the no. 19 and 20 maps along with the figure 22 statistics. From those things we came to know which conversion had the highest coverage. This map tells the story of the inherent process behind these processes by sub-dividing these conversion processes into more detailed division based on the temporal degree of each type conversion occurrence.

5. DISCUSSIONS

5.1. Dynamics of permanent water body, permanent high percentage of vegetated areas

Change of permanent waterbodies from 2016-17 to 2017-18 showed a drastic change of decrease in permanent water bodies. As this study was carried out during post monsoon to pre-monsoon period in this time period usually water starts to decrease in the study area and starts to increase again when the pre-monsoon season comes around which starts from April. Our study period lasts until March hence from April water bodies will start to increase again meaning waterbodies lasting long until March are the permanent water parts of the study area within this time period.

In 2016-17 images the March image was missing because in that month both Landsat and Sentinel-2 images were covered by clouds. This can be another reason for a higher estimation of permanent water body in the image because in March further drying up of the areas occur and the extent change. While integrating maps this has an influence in the output pixel value because in each pixel 1 is identified as water which is the lowest value occurring in the image while calculating the output as maximum. So, may be some areas in 2016-17 image where a higher estimation of permanent water was found that may be those pixels would dry up in the next month and was not included in the output if the image was available.

Another thing to notice is while Sentinel-2 image was missing to fill the gap we used Landsat surface reflectance products with 30 meters resolution to calculate MNDWI and fill the gap. This could also have an influence on the result as when we used this image we needed to resample it to 10 meters meaning the values were resampled to 10 meters from 30 meters which may be creating problems by distributing 30 meters coverage features into 10 meters. Giving erroneous results. Though by visual inspection only a little difference was detected.

For areas of permanent high vegetation area change, there was no data found to validate this result. But these results complement each other, as from figure-x and x shows that while permanent water bodies were lost throughout the study area from 2016-17 to 2017-18, there were many places where high percentage of vegetation cover started to emerge. And these places are basically the places where permanent water bodies were lost during this time period. Hence, retreat of waterbodies may have an influence on the vegetation distribution of vegetation regime.

5.2. Areas covered by different types of cover conversions

During November to December the main process of conversion that dictated throughout the study area was water parts of the study area being changed into soil mixed with water. As November is the first month of post monsoon period hence this can be said that during this period, precipitation stays also a bit lower than the previous months of monsoon. The average seasonal flow also stays a bit lower during this time period (JICA, 2013). So, the places that start losing water in this month may be are those places where depth of water was a bit lower hence with emergence of dry season they start drying up through evaporation. The immediate after dominating conversion process is moist soil being turned into driers soil. Emergence of less precipitation induced season may be the main reason for this. There are also places where water is directly turning into dry soil, this may be happening because of a different type of soil present there.

During December to January the conversion process coverage over the study area kind of followed same trend as both are dry season months, not much difference between temperature or rainfall occurred during those two months 2017-18.

During February to March there was a drastic increase in soil mixed with water to drier soil coverage areas. This is again an indication of irrigation water being extensively used by the farmers there. Also, a lot of Boro cultivation starts there at this period of time (JICA, 2013). This can also be a reason of water mixed with soil being turned into dry soil parts as with agricultural activities starting soil moisture tend to decrease (Zhang & Walsh, 2007).

5.3. Different levels of susceptibility of water dynamics throughout the study area

Figure-22 shows permanent water shown by figure-13 which was calculated from Google Earth Engine has a correspondence with the permanent water depicted in the ILWIS derived temporal conversion process frequency map. The other parts of this maps are named as different levels of susceptibility of conversion process that can happen for many reasons. This map was created by four different days image being summed up together. Four images are of four different months ranging from a wet season (post monsoon) when the area stays inundated, to the dry season when the water in those areas get soaked up. Though one image per month is inappropriate to draw such conclusions of locating features based on water dynamics processes as one image cannot fully reflect the dynamics of whole month (Baret et al., 2006). But because of cloud coverage no images were available except those images there.

The locations and phenomena of susceptibility can be explained from two perspectives, either depth of water or type of soil. Areas which are less conducive to transform into soil moisture that shows that these areas either turn into soil moisture very rarely or maybe they take too much time to turn into soil. But as within 4 months at one image this least susceptible area was soil which indicates that that has already been gone through the process of being turned into soil. So, either this area is dried once within these 4 months as from creeping towards dry season in the middle or it may be the dry season month when it was soil which can very be possible. If that is so, as this area takes during last month of March to turn into soil this area may be a deeper water part which are called beels which retain water during dry months also in Tanguar Haor (TUCN, n.d.). There may be another reason of soil type which is easily eroded away that's why this watery part instead of turning into soil then again turn into water, this would be the case if the conversion phenomena occurred before the dry season i.e. February and March. Another possibility is this place was soil from very before but because of constant erosion this turned into water, this may also happen. In fact, the names that are given to these classes are from one perspective as we don't know what is happening in the other days of the month.

Areas which most often turn into moist soil those may be because of having a shallower depth than the previous one as probability of water to soil conversion is happening here more frequently. Noe this frequency does it have a consistency or sequence that cannot be known from this map, but this can be said that they converted into soil at least two days among the analysis period image days and every image is from different months. Hence, there's possibility that some period before and after of those two days this place has remained soil. So, this place has a higher resistance against turning into water in other words from post monsoon to dry season they follow the natural rule of being dried up. Such places are the transitory parts which on the onset of monsoon or floods, all these go under water, transforming the entire wetland into a single sheet of water, changing the whole scenario. Such places are called Kanda in Tanguar Haor which are intermediate places between permanent water and dry areas.

Areas which always stay moist mainly because of the type of soil present there. And the areas where moist soil sometimes or often turns into dry soil these are function of capacity of different types of soil to carry or store water content (Kramer & Coile, 2008). Another thing is starting of cultivation of vast paddy fields may also be another reason as specially from figure-19 we can see high percentage of vegetation cover areas are mounded on higher elevation areas which usually don't get inundated as the river levees and in the wetland mounds, which very extensively correlates with the locations of dry soil in this map.

5.4. Usage of Google Earth Engine in mapping dynamics of wetlands in the context of this analysis

As a web-based remote sensing platform, Google Earth Engine has proved to be a powerful tool to conduct dynamics analysis in both space and time domain by accessing a wide variety of spatial datasets in one consolidated system. One useful aspect of Google Earth Engine is that the analysis scale is determined by the user meaning output resolution is the resolution of calculation to be carried out. This creates opportunity for using a wide variety of remote sensing products together despite of having different resolutions. In our analysis, for water regime mapping Sentinel-2 data was used. But these datasets were provided without atmospheric correction in Google Earth Engine. This doesn't hinder the path of our objective to look at the water regime dynamics if our objective is to look at the trade-off between water and land state only. But in terms of vegetation mapping Top of atmosphere products usage in terms spectral index calculation can be very erroneous. In Google Earth Engine atmospherically corrected Landsat-8 products were provided which we used for analysis of vegetation mapping which minimized the risk of getting erroneous results. In this way for comprehensive remote sensing of wetlands Google Earth Engine could be a good platform of analysis when it's the question of analysing a large amount of time series data and different types of remote sensing data is the requirements.

The functionality of determining resolution from output is also a bad side of this machine learning platform. Because with every zoom level in the code editor the values continuously get nearest neighbourhood resampling which keep reducing the accuracy. Though for large scale mapping its not a big problem but for small scale mapping this can create erroneous results.

Another capability of Google Earth Engine is its capability of storing a lot of data.in an effective way also providing suitability of calling these datasets through parallel computing procedure. This way very complex calculation over a large amount of remote sensing data can help in calculating results faster.

Histogram representation in Google Earth Engine is another thing that can be improved. We used Google Earth Engine histograms which give only count of pixels as output. This created a lot of problems in our thresholding method. In terms of this QGIS and ILWIS software could be used in a more effective way.

For calculating permanent waterbody separately, we used spatial aggregation of images maximum and minimum algorithms. This gave us permanent features separately but not in one map. It's because Google Earth Engine cannot perform operations in masked pixels and the reclassified images were output of a masking function. Calculation of permanent and ephemeral water features of wetlands were later aggregated in ILWIS to find out the total dynamics in one map. We used java script for our analysis in Google Earth Engine calculations. May be use of Python could improve the methods of working procedure.

6. CONCLUSIONS AND RECOMMENDATIONS

6.1. Conclusions

1. Different thresholds were used for each image. While each image was compared with the Planet derived high resolution images after each time of thresholding it was showing different extents in the derived map. November months thresholds were applied to the December image then the extent derived from the thresholds were compared with corresponding date and time of high-resolution image. It was found that those thresholds were overestimating water features, mixture of a different normal distribution was found also which proved that within the threshold range another type of cover exists. Hence, thresholds were re-adjusted. These levels of re-adjustments linked the real-world behaviour of each month with ranges of MNDWI values. Hence, temporal interpretation of MNDWI ranges interpreted the real world hydrologic and vegetation dynamics.

2. 8.4 km² area of permanent water were lost from the year of 2016-17 to 2017-18. From the perspective of vegetation regime, the amount of high percentage of vegetation cover substantially decreased as high as 14.3 km².

3. During 2016-17 period of year pre-monsoon to post-monsoon land cover conversion coverages mainly can be divided into two portions of the study period. During the immediate after months of post monsoon season i.e. during November to December the conversion process that mostly covered the study area is water to moist soil conversion (30% of the study area). On the other hand, at the last period of the season when the dry season emerges the dominated conversion process over the whole area appear to be moist soil to dry soil (60% of the whole study area.)

4. Mapping of susceptibility of certain places to different types of conversion also provided with a map which can be used for further landscape specific analysis.

5. Using the maximum and minimum algorithms over an image collection permanent and non-permanent areas of water and vegetation part was found out. A sum algorithm in Google Earth Engine could also be used. But separation of permanent water body and non-permanent water parts helped to look at the dynamic's interaction of two regimes and their permanency and non-permanency distinctively. Many other algorithms in Google Erath Engine are provided with respect to more innovative calculations which could be utilized according to research objectives and questions to be achieved.

6.2. Recommendations

1. Validation of reclassified images could be done with accurate field data to assess the accuracy of Google Earth Engine wetland related products which is skipped in this research because of time limitation.
2. Vegetation regime dynamics could be more extensively recorded through the Sentinel-1 Synthetic Aperture Radar data and integrating with the optical based analysis this information could be linked with susceptibility map or the landcover conversion map to further investigate deeper between the relationship of vegetation and hydrologic regime of wetlands.
3. Google Earth Engine based phenological model or linear regression models can be used for looking at the dynamics from different perspectives along with hydrological regime to assess the effectiveness of GEE algorithms in terms of wetland dynamics which because of time limitation is skipped in this research.
4. There's a new tool emerging for quantifying and analysing the dynamics of changing cover of earth recently been invented known as Earth Engine Digitisation Tool which can be utilized to assess the changes in wetlands.

7. LIST OF REFERENCES

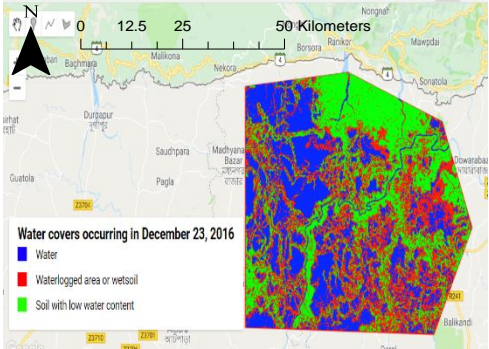
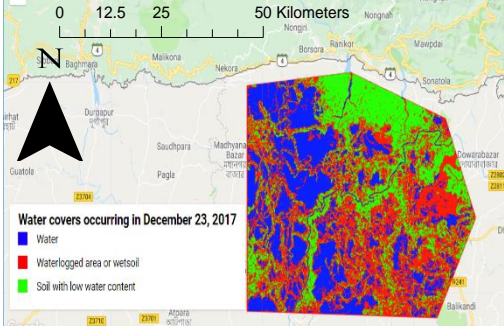
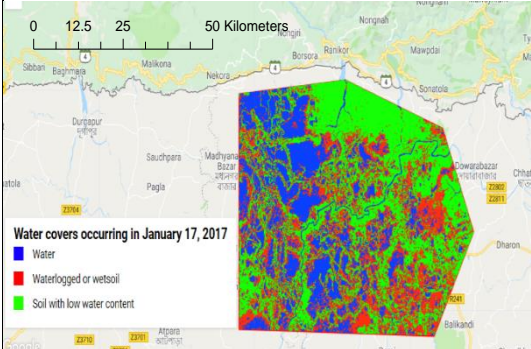
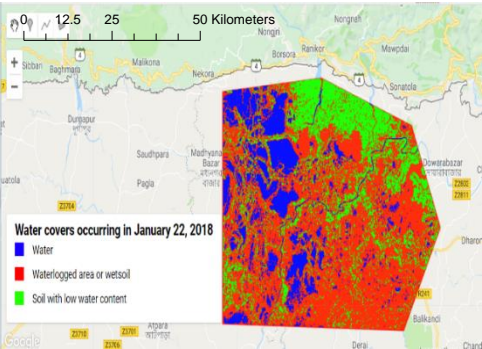
- A. R. HUETE. (1988). A Soil-Adjusted Vegetation Index (SAVI), *309*, 295–309.
- Alonso, A., Kennedy, R. E., & Murcia, C. (2016). wetland landscape spatio-temporal degradation dynamics using the new google earth engine cloud-based platform: opportunities for non-specialists in remote sensing, *59*, 1333–1344. <https://doi.org/10.13031/trans.59.11608>
- Bannari, A., Morin, D., Bonn, F., & Huete, A. R. (1995). A review of vegetation indices. *Remote Sensing Reviews*, *13*(1–2), 95–120. <https://doi.org/10.1080/02757259509532298>
- Baret, F., Bartholomé, E., Bicheron, P., Borstlap, G., Bydekerke, L., Combal, B., ... Roey, T. Van. (2006). VGT4Africa user manual First edition, 256.
- CEGIS. (2012). Master Plan of Haor Area, Volume II: Main Report, II, 73–80.
- Chandra, R. (2017). *Wetland Science*. <https://doi.org/10.1007/978-81-322-3715-0>
- Comer, P. J., Faber, D., Menard, S., Connor, O., Higman, P., & Man, Y. (n.d.). User Guide for Wetland Assessment and Monitoring in Natural Resource Damage Assessment and Restoration.
- Dörnhöfer, K., Göritz, A., Gege, P., Pflug, B., & Oppelt, N. (2016). Water constituents and water depth retrieval from Sentinel-2A-A first evaluation in an oligotrophic lake. *Remote Sensing*, *8*(11). <https://doi.org/10.3390/rs8110941>
- Du, Y., Zhang, Y., Ling, F., Wang, Q., Li, W., & Li, X. (2016). Water bodies' mapping from Sentinel-2 imagery with Modified Normalized Difference Water Index at 10-m spatial resolution produced by sharpening the swir band. *Remote Sensing*, *8*(4). <https://doi.org/10.3390/rs8040354>
- Gervasi, O., Murgante, B., Misra, S., Stankova, E., Torre, C. M., Maria, A., ... Hutchison, D. (2018). *and Its Applications – ICCSA 2018*. <https://doi.org/10.1007/978-3-319-95162-1>
- Gorelick, N., Hancher, M., Dixon, M., Ilyushchenko, S., Thau, D., & Moore, R. (2017). Google Earth Engine: Planetary-scale geospatial analysis for everyone. *Remote Sensing of Environment*, *202*, 18–27. <https://doi.org/10.1016/j.rse.2017.06.031>
- Guo, M., Li, J., Sheng, C., Xu, J., & Wu, L. (2017). A review of wetland remote sensing. *Sensors (Switzerland)*, *17*(4), 1–36. <https://doi.org/10.3390/s17040777>
- Han, J., Wei, C., Chen, Y., Liu, W., Song, P., Zhang, D., ... Huang, J. (2017). Mapping above-ground biomass of winter oilseed rape using high spatial resolution satellite data at parcel scale under waterlogging conditions. *Remote Sensing*, *9*(3). <https://doi.org/10.3390/rs9030238>
- Haque, M. I., & Basak, R. (2017). Land cover change detection using GIS and remote sensing techniques: A spatio-temporal study on Tanguar Haor, Sunamganj, Bangladesh. *Egyptian Journal of Remote Sensing and Space Science*, *20*(2), 251–263. <https://doi.org/10.1016/j.ejrs.2016.12.003>
- Hird, J. N., Delancey, E. R., & Mcdermid, G. J. (2017). Google Earth Engine , Open-Access Satellite Data , and Machine Learning in Support of Large-Area Probabilistic Wetland Mapping, *d*(iii). <https://doi.org/10.3390/rs9121315>
- Huang, C., Chen, Y., Zhang, S., & Wu, J. (2018). Detecting, Extracting, and Monitoring Surface Water From Space Using Optical Sensors: A Review. *Reviews of Geophysics*, *56*(2), 333–360. <https://doi.org/10.1029/2018RG000598>
- Huete, A. R. (1992). Soil Optical Properties And Environmental Applications Of Remote Sensing. *Japanese Society of Biofeedback Research*, *19*, 709–715. https://doi.org/10.20595/jjbf.19.0_3
- Information Sheet on Ramsar Wetlands (RIS). (2000), (50), 1–8.
- jica, (2013). data collection survey on water resources management in haor area of bangladesh data collection survey on water resources management in, (December).
- Kabisch, N., Selsam, P., Kirsten, T., Lausch, A., & Bumberger, J. (2019). A multi-sensor and multi-temporal remote sensing approach to detect land cover change dynamics in heterogeneous urban landscapes. *Ecological Indicators*, *99*(July 2018), 273–282. <https://doi.org/10.1016/j.ecolind.2018.12.033>
- Kaplan, G., Avdan, & Leeuwen, V. (2017). MAPPING AND MONITORING WETLANDS USING SENTINEL-2 SATELLITE IMAGERY, *IV*(October), 14–15.
- Karim, A., Rashid, S. M. A., Sobhan, I., & Mahmud, S. (n.d.). “TANGUA HAOR”, Ramsar Site , Wetlands Gene Bank of, 1–16.
- Kramer, P. J., & Coile, T. S. (2008). an Estimation of the Volume of Water Made Available By Root Extension. *Plant Physiology*, *15*(4), 743–747. <https://doi.org/10.1104/pp.15.4.743>

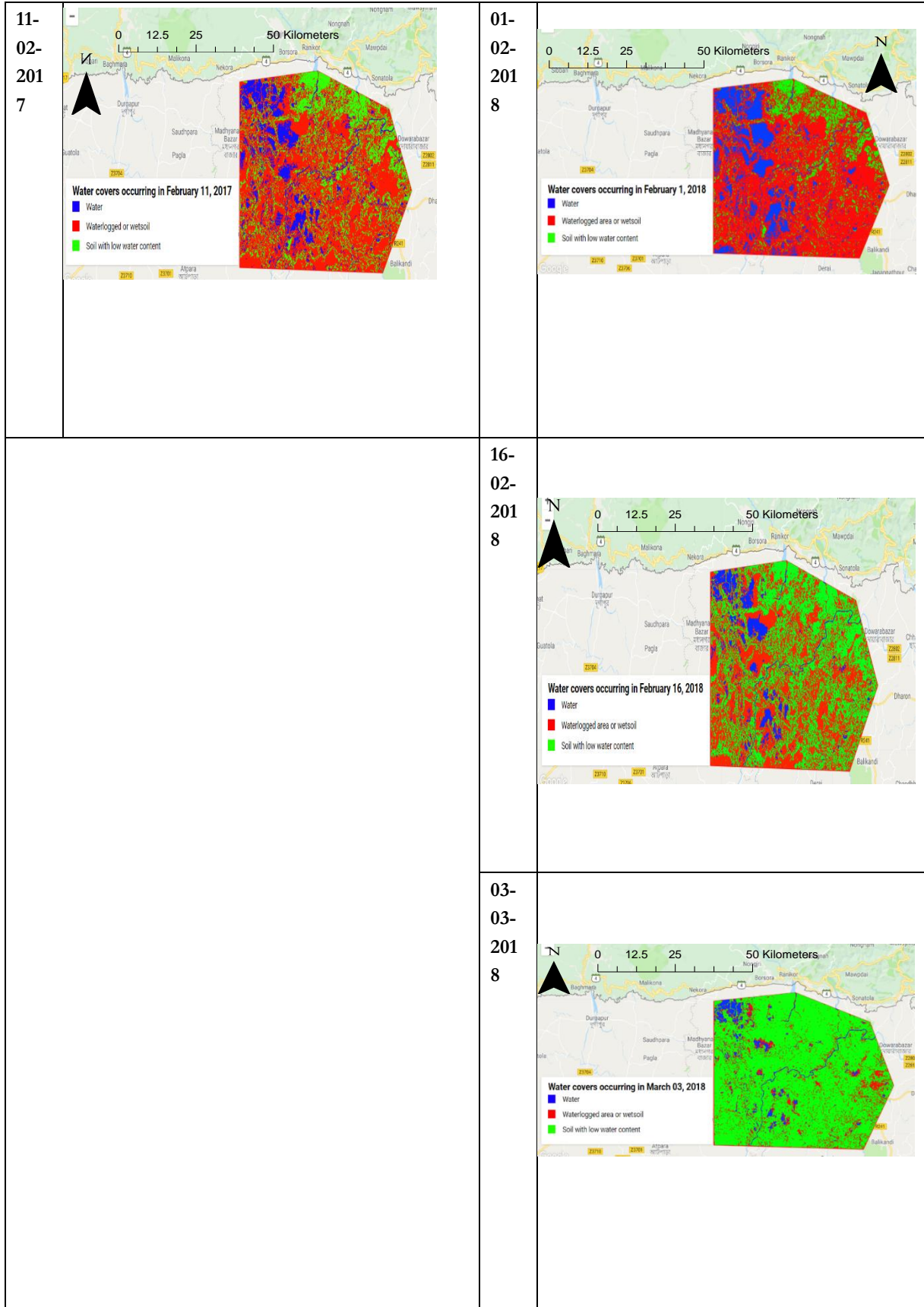
- Ma, S., Zhou, Y., Gowda, P. H., Dong, J., Zhang, G., Kakani, V. G., ... Jiang, W. (2019). Application of the water-related spectral reflectance indices: A review. *Ecological Indicators*, 98(May 2018), 68–79. <https://doi.org/10.1016/j.ecolind.2018.10.049>
- Mahdianpari, M., Salehi, B., Mohammadimanesh, F., Homayouni, S., Gill, E., Mahdianpari, M., ... Gill, E. (2018). The First Wetland Inventory Map of Newfoundland at a Spatial Resolution of 10 m Using Sentinel-1 and Sentinel-2 Data on the Google Earth Engine Cloud Computing Platform. *Remote Sensing*, 11(1), 43. <https://doi.org/10.3390/rs11010043>
- Masilūnas, D., Verbesselt, J., & Pena-Claros, M. (2017). Evaluating the potential of Sentinel-2 and Landsat image time series for detecting selective logging in the Amazon.
- Miah, M. G. U., Afrad, M. S. I., Mehraj, H., & Mandal, M. S. H. (2015). Land Use Change and Its Impact on Ecosystem Services, Livelihood in Tanguar Haor Wetland of Bangladesh. *Scientia Agriculturae*, 12(2). <https://doi.org/10.15192/PSCP.SA.2015.12.2.7888>
- Midekisa, A., Holl, F., Savory, D. J., Andrade-Pacheco, R., Gething, P. W., Bennett, A., & Sturrock, H. J. W. (2017). Mapping land cover change over continental Africa using Landsat and Google Earth Engine cloud computing. *PLoS ONE*, 12(9), 1–15. <https://doi.org/10.1371/journal.pone.0184926>
- Mitsch, W. J., & Gosselink, J. G. (n.d.). *No Title*.
- Muñoz, A.-R., Wang, T., Vrieling, A., Skidmore, A., Turak, E., & Li, L. (2015). Evaluation of MODIS Spectral Indices for Monitoring Hydrological Dynamics of a Small, Seasonally-Flooded Wetland in Southern Spain. *Wetlands*, 35(5), 851–864. <https://doi.org/10.1007/s13157-015-0676-9>
- Murat, K., & Ceylan, N. (2005). The Spectral Reflectance Responses of Water with Different Levels. *Turkish Journal Engineering and Environmental Sciences*, 29(January), 351–360.
- Muzaffar, S. B., & Ahmed, F. A. (2007). The effects of the flood cycle on the diversity and composition of the phytoplankton community of a seasonally flooded Ramsar wetland in Bangladesh. *Wetlands Ecology and Management*, 15(2), 81–93. <https://doi.org/10.1007/s11273-006-9014-6>
- Nagler, P. L., Glenn, E. P., & Huete, A. R. (2001). Assessment of spectral vegetation indices for riparian vegetation in the Colorado River delta, Mexico, 91–110. <https://doi.org/10.1006/jare.2001.0844>
- Nhamo, L., Magidi, J., & Dickens, C. (2017). Determining wetland spatial extent and seasonal variations of the inundated area using multispectral remote sensing. *ISSNOnline = Water SA*, 43(4), 1816–1950. <https://doi.org/10.4314/wsa.v43i4.02>
- Papa, F., Prigent, C., Durand, F., & Rossow, W. B. (2006). Wetland dynamics using a suite of satellite observations: A case study of application and evaluation for the Indian Subcontinent, 33(August), 2–5. <https://doi.org/10.1029/2006GL025767>
- Resources, N. (n.d.). of Remote Sensing Fundamentals.
- Rondeaux, G., Steven, M., & Baret, F. (1996). Optimization of Soil-Adjusted Vegetation Indices, 107(August 1994), 95–107.
- Sidhu, N., Pebesma, E., & Câmara, G. (2018). Using Google Earth Engine to detect land cover change: Singapore as a use case. *European Journal of Remote Sensing*, 51(1), 486–500. <https://doi.org/10.1080/22797254.2018.1451782>
- Silleos, N. G., Alexandridis, T. K., Gitas, I. Z., & Perakis, K. (2006). Vegetation indices: Advances made in biomass estimation and vegetation monitoring in the last 30 years. *Geocarto International*, 21(4), 21–28. <https://doi.org/10.1080/10106040608542399>
- Singh, K. V., Prasad, A., Pateriya, B., Sahoo, S., & Setia, R. (2014). Evaluation of NDWI and MNDWI for assessment of waterlogging by integrating digital elevation model and groundwater level. *Geocarto International*, 30(6), 650–661. <https://doi.org/10.1080/10106049.2014.965757>
- Sutter, L. A. (2014). watershed-based wetland, (August 2000).
- Tang, W., & Feng, W. (2017). Parallel map projection of vector-based big spatial data: Coupling cloud computing with graphics processing units. *Computers, Environment and Urban Systems*, 61, 187–197. <https://doi.org/10.1016/j.compenvurbsys.2014.01.001>
- Tanguar Haor Management Plan Framework and Guidelines. (n.d.).
- Wang, P., Wang, J., Chen, Y., & Ni, G. (2013). Rapid processing of remote sensing images based on cloud computing. *Future Generation Computer Systems*, 29(8), 1963–1968. <https://doi.org/10.1016/j.future.2013.05.002>
- White, L., Brisco, B., Daboor, M., Schmitt, A., & Pratt, A. (2015). *A collection of SAR methodologies for monitoring wetlands. Remote Sensing* (Vol. 7). <https://doi.org/10.3390/rs70607615>
- Wu, Q. (2017). GIS and Remote Sensing Applications in Wetland Mapping and Monitoring. *Comprehensive Geographic Information Systems*, (April), 140–157. <https://doi.org/10.1016/b978-0-12-409548-9.10460-9>
- Xue, J., & Su, B. (2017). Significant Remote Sensing Vegetation Indices: A Review of Developments and

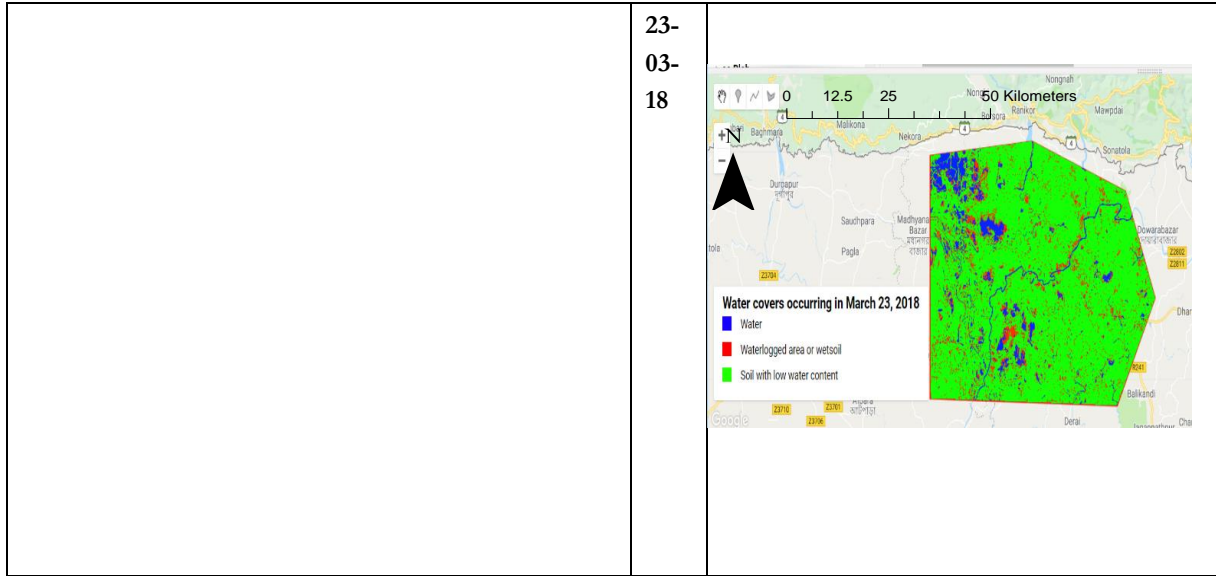
- Applications. *Journal of Sensors*, 2017, 1–17. <https://doi.org/10.1155/2017/1353691>
- Yang, C., Yu, M., Hu, F., Jiang, Y., & Li, Y. (2017). Utilizing Cloud Computing to address big geospatial data challenges. *Computers, Environment and Urban Systems*, 61, 120–128. <https://doi.org/10.1016/j.compenvurbsys.2016.10.010>
- Yuan, L. H., Jiang, W. G., Luo, Z. L., He, X. H., & Liu, Y. H. (2014). Analysis of wetland change in the Songhua River Basin from 1995 to 2008. *IOP Conference Series: Earth and Environmental Science*, 17(1). <https://doi.org/10.1088/1755-1315/17/1/012125>
- Zhang, J., & Walsh, J. E. (2007). Relative impacts of vegetation coverage and leaf area index on climate change in a greener north, 34(June), 1–6. <https://doi.org/10.1029/2007GL030852>

APPENDIX

Appendix 1: Reclassified MNDWI images

| Date | MNDWI reclassified maps 2016-17 | MNDWI reclassified maps 2017-18 |
|------------|---|--|
| 23-12-2016 |  |  |
| 17-01-2017 |  |  |

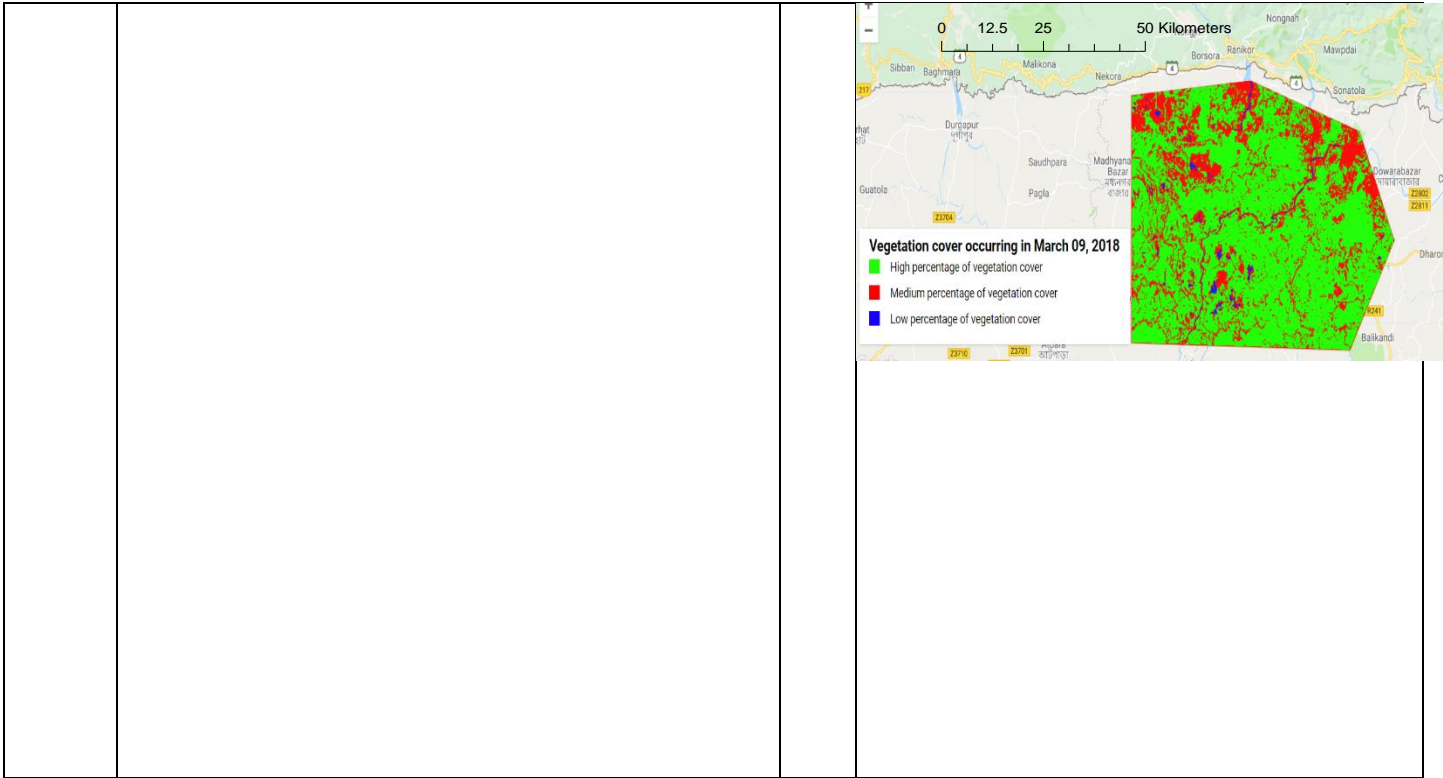




Appendix 2 Reclassified SAVI images

| Date | SAVI reclassified maps 2016-17 | SAVI reclassified maps 2017-18 |
|-------------------|--------------------------------|--------------------------------|
| <p>2016-11-14</p> | | <p>2017-11-03</p> |





Appendix 3: Example of codes to generate one full MNDWI and SAVI calculation

MNDWI for 13-11-2016

```

var tanguarhaor = ee.Geometry.Polygon([
[[91.02, 25.16], [91.26,25.18],[91.48,25.11],[91.55, 24.96], [91.46, 24.81], [91.02, 24.82],[91.02,25.16]]]);
Map.centerObject(tanguarhaor);
Map.addLayer(tanguarhaor, {color: 'FF0000'}, 'geodesic polygon');
print('Polygon area: ', tanguarhaor.area().multiply(0.0001));
print ('Polygon area: ', tanguarhaor.area().multiply(0.0001))
//print ('Polygon area: ', geometry17.length())//.multiply(0.0001))
var qax1 =
(ee.Image('COPERNICUS/S2/20161113T043032_20161113T043537_T46RCN')).select('QA60')//.get('
CLOUDY_PIXEL_PERCENTAGE')
var cloudBitMask = 1 << 10;
var cirrusBitMask = 1 << 11;
var maskx1 = qax1.bitwiseAnd(cloudBitMask).eq(0).and(
qax1.bitwiseAnd(cirrusBitMask).eq(0));
var qax2 =
(ee.Image('COPERNICUS/S2/20161113T043032_20161113T043537_T46RCN')).updateMask(maskx1).
divide(10000).clip(tanguarhaor).unmask(0)
var band1y = qax2.select('B11');
var band2y = qax2.select('B3');
//print('CRS:', band2.projection().crs());
// Display a bilinear resampled image with 10m pixel spacing.
var image_10mk = band1y.resample('bilinear').reproject({
crs: band2y.projection().crs(),
scale: 10
});
//Map.addLayer(image_10m, {min:0, max: 0.3});
var mndwinovemberk = (qax2.select('B3').subtract(image_10mk.select('B11')))
.divide((qax2.select('B3')).add(image_10mk.select('B11')));
//Map.addLayer( mndwinovember,
// {min:0, max: 1});
var image1 = ee.Image(1)
var image2 = ee.Image(2)
var image3 = ee.Image(3)
var image4 = ee.Image(4)
//Map.addLayer( image3,
// {min:0, max: 1}); 75

```

```

var waterreclass1617 = ( water1617.where(( water1617.gt(0.6)).or( water1617.eq(0.6)), image1))
var waterloggedwithvegnov1617 =
(mndwinovemberk.lt(0.6)).and(mndwinovemberk.gt(0)).or(mndwinovemberk.eq(0))
var waterloggedvegnovmask1617 = mndwinovemberk.mask( waterloggedwithvegnov1617 )
var waterloggedwithvegnovclass1617 = ( waterloggedvegnovmask1617.where((
waterloggedvegnovmask1617.lt(0.6)).and(( waterloggedvegnovmask1617.gt(0)).or(
waterloggedvegnovmask1617.eq(0))),image2))
var nonwater1617 = (mndwinovemberk.lt(0))
var nonwatermask1617 = mndwinovemberk.mask(nonwater1617)
var nonwaterclass1617 = (nonwatermask1617.where((nonwatermask1617.lt(0)),image3))
var novemberreclassified1617 = ee.ImageCollection ([ waterreclass1617,
waterloggedwithvegnovclass1617,nonwaterclass1617]).mosaic()
//Map.addLayer( novemberreclassified1617,
// {min:1, max: 3});
SAVI calculation – 2016-14-11
var qax16 =
(ee.Image('LANDSAT/LC08/C01/T1_SR/LC08_137043_20161114')).divide(3000).clip(tanguarhaor)
var xy3 =
((qax16.select('B5')).subtract(qax16.select('B4'))).multiply(1.5)//.divide((qa1.select('B8')).add(pansharpen1.
select('B11')).subtract(pansharpen1.select('B12')));
var xy4 = (qax16.select('B5').add(qax16.select('B4')).add(0.5))
var SAVIq2 = xy3.divide(xy4)
var thresholdq4 = ( SAVIq2.gt(0.4)).or( SAVIq2.eq(0.4))
var thresholdq5 = ( SAVIq2.lt(0.4)).and( SAVIq2.gt(0)).or( SAVIq2.eq(0))
var thresholdq6 = ( SAVIq2.lt(0)).or( SAVIq2.eq(0))
var highdensityq4 = SAVIq2.mask(thresholdq4)
var mediumdensityq5 = SAVIq2.mask(thresholdq5)
var lowdensityq6 = SAVIq2.mask(thresholdq6)
var highdensityvegreclass1617a =
highdensityq4.where((highdensityq4.gt(0.4)).or(highdensityq4.eq(0.4)),image1)
var mediumdensityvegreclass1617a = ( mediumdensityq5.where(( mediumdensityq5.lt(0.4)).and((
mediumdensityq5.gt(0)).or( mediumdensityq5.eq(0))),image2))
var lowdensityveg1617cclassa = (lowdensityq6.where((lowdensityq6.lt(0)),image3))
var reclassifiedvegnovember1617e = ee.ImageCollection ([highdensityvegreclass1617a ,
mediumdensityvegreclass1617a ,lowdensityveg1617cclassa]).mosaic()
// Map.addLayer(reclassifiedvegnovember1617e, {min:1, max: 3});

```